Ref. Ares(2022)3518929 - 07/05/2022

Funded by European Union Civil Protection
Grant Agreement Number 874421

Vulnerability assessment of embankments and bridges exposed to flooding hazards

D4.1 Report on Vulnerability Assessment Methodology - Fragility curves for embankments subjected to flooding

Project Information

Grant Agreement No.	874421
Project Acronym	oVERFLOw
Project Full Title	Vulnerability assessment of embankments and bridges exposed to flooding hazards
Starting Date	1 December 2019
Duration	32 months
Call Identifier	UCPM-2019-PP-AG
Topic	UCPM-2019-PP-PREV-AG: Prevention in civil protection and marine pollution
Project Website	www.projectoverflow.eu
Project Coordinator	Prof. Meho Sasa Kovacevic
Organisation	Faculty of Civil Engineering, University of Zagreb
E-mail	msk@grad.hr
Telephone	+385 (1) 4639 250

Partner Information

Sveuciliste u Zagrebu Gradevinski Fakultet	Croatia
Infra Plan Konzalting	Croatia
GEKOM - geofizikalno i ekološko modeliranje d.o.o.	Croatia
VEILIGHEIDSREGIO ZUID-HOLLAND ZUID	Netherlands
INGEO BV	Netherlands
ZAVOD ZA GRADBENISTVO SLOVENIJE	Slovenia
Uprava Republike Slovenije za zaščito in reševanje	Slovenia

Document Information

Work Package	**4**
Deliverable Title	Report on Vulnerability Assessment Methodology - Fragility curves for embankments subjected to flooding
Version	1.0
Date of Submission	07/05/2022
Main Editor(s)	Kenneth Gavin, Cormac Reale
Contributor(s)	Mario Bacic, Meho Sasa Kovacevic, Aryan Gupta
Reviewer(s)	Irina Stipanovic, Lovorka Libric
Citation	K. Gavin, C. Reale (2021). oVERFLOw Deliverable 4.1 D4.1 Report on Vulnerability Assessment Methodology - Fragility curves for embankments subjected to flooding

Document Classification:									
Draft		Final	**X**	Confidential		Restricted		Public	**X**

History			
Version	**Issue Date**	**Status**	**Distribution**
1	15/02/2022	Draft	IPK
2	01/05/2022	Final	All partners

The information contained in this report reflects the views of the Author(s) and the Commission does not accept responsibility for the use of this information.

Executive Summary

Floods are a natural phenomenon that can have a significant impact to human-life, ecosystems, cultural heritage and society in general. The three partner countries in the oVERFLOw project, namely Croatia, Netherlands and Slovenia, are particularly vulnerable to cross-border river flooding due to their position near the end of major European river systems. The Netherlands is the most flood prone country in the EU. In response the country built strategic large flood defence schemes and developed a sophisticated flood risk management system for levees. Croatia and Slovenia have joint transboundary river basins, a similar infrastructure and risk management approach regarding flood protection measures, while they are both facing increased flood risks caused by climate change impacts.

Two areas have been chosen as pilot sites, for the deployment and demonstration of the technology developed within the oVERFLOw project. One area is in the Netherlands around the city of Dordrecht (dike rings 16 and 17) and the other area is the city of Karlovac in Croatia. This deliverable presents a methodology for generating fragility curves for assessing the integrity of dykes or levees. These curves explicitly account for both material and loading uncertainty and can be used to interpret how likely a failure is given a flood event. The methodology is applied to the Dutch case study site at Oostmolendijk on the outskirts of Dordrecht and on riverbanks in the city of Karlovac in Croatia.

Keywords: flood events, high water level, fragility curves, levee, riverbank

Table of Contents

Project Information 1
Partner Information 1
Document Information 2
Executive Summary 3
Abbreviations and Acronyms 5
1 Introduction 6
1.1 Overview of the oVERFLOw Project 6
1.2 Overview of Deliverable D4.1 6
2 Modelling Embankment and Riverbank Failure Mechanisms 8
2.1 Global Stability 8
2.2 Rapid Drawdown 8
2.3 Overtopping 8
2.4 Piping 9
2.5 Seismic stability 10
3 Determining Soil Strength 11
3.1 CPT-based Method 11
3.2 SHANSEP FRAMEWORK 12
4 Reliability Analysis 13
4.1 System probability of failure 14
4.2 Describing Geotechnical Uncertainty 15
4.3 Uncertainty in Soil Properties 16
4.4 Fragility Curve Generation 16
4.5 Target Reliability 16
5 Dutch case study - Oostmolendijk 18
5.1 Site Overview 18
5.2 Dyke Geometry 19
5.3 Geotechnical Interpretation 21
5.3 Fragility Curves 29
5.3.2 Global Instability and Overtopping Fragility Curve 33
5.3.3 Rapid Drawdown Fragility Curve 34
5.3.4 System probability of failure curve 34
5.4 Consider of other cross-sections at Oostmolendijk 36
6 Croatian case study – riverbanks in Karlovac 41
6.3.1 Site Overview 41
6.3.2 Selection of the relevant cross sections for analysis 42
6.3.3 Selection of the soil parameters 44
6.3.3 Development of the fragility curves for identified zones 46
7 Conclusion 58
8 References 60

Abbreviations and Acronyms

Abbreviation / Acronym	Description
CAU	CONSOLIDATED ANISOTROPICALLY UNDRAINED TRIAXIAL TEST
CPA	CIVIL PROTECTION AGENCY
CPT	CONE PENETRATION TEST
DSS	DIRECT SIMPLE SHEAR
ERT	ELECTRICAL TOMOGRAPHY
IM	INFRASTRUCTURE MANAGER
MASW	MULTICHANNEL ANALYSIS OF SURFACE WAVES
SHANSEP	STRESS HISTORY AND NORMALIZED SOIL ENGINEERING PROPERTIES
SPT	STANDARD PENETRATION TEST
UAV	UNMANNED AERIAL VEHICLE
VNK2	VEILIGHEID NEDERLAND IN KAART (SAFETY OF THE NETHERLANDS ON THE MAP)
WP	WORK PACKAGE

1 Introduction

1.1 Overview of the oVERFLOw Project

Flooding is a significant threat to human-life, ecosystems, cultural heritage and society in general. The three partner countries in the oVERFLOW project are particularly vulnerable to cross-border flooding from major European river systems. The risk based method for assessing flood defences, the so called VNK2 method, developed in the Netherlands is the state of the art, but the determination of the probability of failure is critically dependent on a number of highly uncertain parameters. The probability of failure is a comparison of the resistance (strength of the system) to the load (in this case a flood event). The most significant uncertainties relate to length effects and the location of potential seepage events in the flood defence systems (affecting the dike strength) and the severity of a flood event.

The overall objective of the oVERFLOw project is to strengthen the resilience of dikes to climate change impacts with the specific objective being the development of climate-resilient infrastructure. This will be achieved by:

- Reducing the known uncertainties in the VNK2 approach using techniques and procedures developed by the applicants in recent H2020 projects to provide real-time response of a critical infrastructure object (levee of bridge) during a flood event.
- The technology will be deployed and demonstrated at two pilot sites, at flood prone areas in the Netherlands and Croatia.

1.2 Overview of Deliverable D4.1

Flood defences are of critical importance for the protection of low-lying areas that would otherwise be threatened by floods. Nowhere exemplifies this more than The Netherlands, where 60% of the country, by area, is at risk of flooding. Unfortunately, most of the country's major cities lie within this zone, placing the majority of the population at risk should flood defences fail. To prevent this from occurring The Netherlands has installed 3800 km of flood defences. Naturally given their risk profile maintaining and managing these flood defences is of utmost importance in The Netherlands (Rijkswaterstaat, 2014). The Croatian city of Karlovac is situated at the intersection of four rivers the Kupa, Korana, Dobra and Mrežnica making it unusually susceptible to flooding. The city is vital to the area's economy providing the main transport link between the coastal cities of Rijeka and Split as well as being an area of significant cultural value. Protecting Karlovac from future flood events is therefore a high priority in Croatia. According to IPCC projections many countries will be exposed to higher peak river discharges in the near future, leading to larger peak surges increasing the chance of catastrophic flood defence failure.

This deliverable describes how to generate fragility curves to examine how vulnerable dykes are to flood events. To accomplish this, significant sections of the report are dedicated to covering aspects of soil variability, reliability and the underlying physics. Several failure

mechanisms are considered in this report namely overall stability, rapid drawdown, piping and overtopping. Two case studies; Oostmolendilk, a primary dyke situated just outside Dordrecht in the Netherlands and Karlovac riverbanks are then analysed in depth and fragility curves are produced for each limit state with event trees used to quantify the system probability of failure.

2 Modelling Embankment and Riverbank Failure Mechanisms

Dykes and riverbanks can fail through a variety of different mechanisms, this project will explicitly consider five different mechanisms namely global stability, overtopping, piping, rapid drawdown and seismic induced instability.

2.1 Global Stability

A variety of Limit Equilibrium Methods exist to determine global stability. Typically these methods are based upon the method of slices, where the sliding volume is subdivided into a predetermined number of vertical slices (or columns in 3D) with forces and or moment equilibrium considered at the boundaries. By summing the weight of material in a slice or a column one can evaluate the normal stress and subsequent shear stress in the slice at a given depth. The minimum factor of safety (FoS) of the slope, defined as its capacity divided by its demand (See Equation 1), is then found by varying the location of the slip surface until the global minimum is found. Prominent examples of slice based methods include Bishop (1955), Janbu (1975), Spencer (1967), Morgenstern & Price (1965) and the General Equilibrium Method (1992). The FOS in global stability terms is defined as the ratio of resisting soil shear strength (capacity) to the shear stress required to initiate mobilisation (demand). An extensive review of Limit Equilibrium Methods (LEMs) suitable for slope stability analysis can be found in Fredlund and Krahn (1977). This report will utilise the Morgenstern and Price (1965) method. However it is important to note, that any of the LEM models discussed above can be adapted for probabilistic analysis.

$$\text{FOS} = \frac{\text{Capacity}}{\text{Demand}} \qquad [1]$$

2.2 Rapid Drawdown

Rapid drawdown failures occur when the water level on the river side of the slope experiences a rapid reduction in level, after a flood event. This is a commonly occurring failure mechanism in river levees and riverbanks as external water levels can drop rapidly whilst the soil in the slope remains fully saturated.

2.3 Overtopping

Overtopping failures occur when as the name suggests water flows over the top of the embankment or levee. For this to occur the flood level has to be larger than the height of the dyke which makes this a very unlikely failure mechanism in the majority of well-designed flood defences, nevertheless it remains a possibility during extreme events. If overtopping

were to occur the water velocity will increase down the landside slope of the embankment until such time as the water momentum and slope frictional resistance equilibrate and the flow reaches a steady state. This can be modelled as an additional shear stress imparted to the landslide slope surface (Rossi *et al.*, 2021). The velocity at which flow becomes steady state can be calculated using the following equation:

$$v_0 = \left(\frac{\sqrt{\sin\alpha}}{n}\right)^{\frac{3}{5}} q_0^{\frac{2}{5}} \quad [2]$$

Where v_0(m/s) is the steady state velocity down the slope, α is the slope angle, n is Manning's coefficient and q_0 is the steady discharge. A Manning's coefficient of 0.02 is recommended for slopes of 1:3. The discharge over the levee crown can be calculated using the equation for flow over a broad crown weir (Rossi *et al.*, 2021).

$$q = \left(\frac{2}{3}\right)^{1.5} \sqrt{g} h_1^{1.5} \quad [3]$$

Where g represents gravity and h_1 is the height of the discharge at the crest of the slope. At steady flow, discharge is constant along the slope therefore the height of water perpendicular to the slope can be obtained from

$$h = \frac{q}{v_0} \quad [4]$$

The applied shear stress, $\boldsymbol{\tau_0}$ from the surge overflow can then be calculated from:

$$\tau_0 = \gamma_w h \sin\alpha \quad [5]$$

Where the unit weight of water is γ_w.

2.4 Piping

Piping occurs when particles within or below the levee are eroded due to seepage. If seepage forces become large enough particles can get washed out of the soil, promoting increased flow which in turn can wash away larger particles and create a channel or a "pipe". This channel works its way from the interior to the exterior of the dam, at which point the dyke is breached as there is a continuous erosion channel allowing water to freely flow from one side of the dam to the other. The speed at which this occurs is controlled by the pore pressure and the permeability of the material.

Piping has been modelled in this report using Sellmeijers equations, which are a series of equations resulting from combining empirical relations from lab experiments and field observations with an underlying physical model. The model calculates the critical head difference ΔH_c $[m]$, which is the largest head difference that can be sustained before piping occurs. It can be calculated from Equation 6. If the change in pressure head ΔH is greater than ΔH_c then failure occurs.

$$\Delta H_c = F_r F_s F_g L \quad [6]$$

where L is the length of the seepage path [m], F_r, F_s and F_g are dimensionless terms describing the resistance scale and geometry. Equations 7-9 can be used to calculate these terms.

$$F_r = \eta \tan\theta \frac{\gamma_b'}{\gamma_w} \quad [7]$$

$$F_s = \frac{d_{70,m}}{\sqrt[3]{\kappa L}} \left(\frac{d_{70}}{d_{70,m}}\right)^{0.4} \quad [8]$$

$$F_g = 0.91 \left(\frac{D}{L}\right)^{a} \quad [9]$$

where $a = \frac{0.28}{\left(\frac{D}{L}\right)^{2.8} - 1} + 0.04$, D [m] is the thickness of the sand land layer, d_{70} [m] is the 70th percentile of the grain size distribution of the sand, $d_{70,m}$ [m] is a reference value typically taken as 0.0002, κ [m^2] is the intrinsic permeability, θ is the bedding angle, η is White's constant, γ_b' [kN/m^3] is the effective soil unit weight and γ_w is the unit weight [kN/m^3] of water.

The piping limit state is described in Equation 10.

$$G(X) = \Delta H_c - \Delta H \quad [10]$$

2.5 Seismic stability

Earthquake induced shaking can also cause of levee and riverbank failure. Static slope stability is dependent on several factors such as geometry, soil type, ground water level, permanent and transient actions. In addition, dynamic slope stability needs to consider how shear strength changes during cyclic actions and as inertia loads increase. Two possible approaches can be used for evaluation of the slope stability under seismic conditions, the first approach analyses permanent deformation using the Newmark's sliding block approach (Newmark, 1965), the second approach developed by Terzaghi (1950) considers pseudo-static stability based using a factor of safety concept. This study uses the latter one, where the complex soil shaking is replaced with constant pseudo-static acceleration acting in one direction.

3 Determining Soil Strength

Dutch design regulations state that the undrained shear strength, s_u determined using the SHANSHEP approach should be used to for the stability analyses of a Dyke section subject to flooding. Because of the difficulty in obtaining high-quality test samples and the natural variability of soils in many parts of the world it is common to estimate s_u using correlations with in-situ test results. The Cone Penetration Test (CPT) is widely used to characterise the response of soft deltaic soils and sand deposits. This report will calculate the undrained shear strength using both CPT-based method and the SHANSEP method.

3.1 CPT-based Method

To derive a soils undrained shear strength using in-situ CPTu data, a site-specific transformation factor (N_{kt}) is used to relate the results of undrained laboratory strength tests at discrete locations to CPT tip resistance data. To calibrate the method, soil samples need to be acquired and tested from a borehole adjacent to the CPT. An appropriate project specific N_{kt} value for each soil type can be determined with the help of a shear strength test such as a direct simple shear or triaxial test. This N_{kt} value can be then used to calculate the Undrained Strength at nearby CPT locations.

The calculation of undrained shear strength from CPTu data is achieved through the following equations.

$$s_u = \frac{q_t - \sigma_{v0}}{N_{kt}} \quad [11]$$

where

$$q_t = q_c + (1 - \alpha)u_2 \quad [12]$$

where N_{kt} is an empirical correlation factor, σ_{v0} is the total vertical stress, q_t is the corrected tip resistance, q_c is the measured CPT tip resistance, u_2 is the pore pressure measured behind the cone shoulder (u_2) position and α is the cone's alpha factor (typically equal to 0.15). The measured undrained shear strength (s_u) is compared with the net cone resistance q_{net} of the CPT at approximately the same location and depth.

The strain levels used to determine s_u depend on the soil type and test method. In the SHANSHEP method clays are tested in the triaxial cell, whilst peats are tested in the direct shear test. The defined critical state strain levels are 25% and 40% in the trixial and direct shear test devices respectively.

Multiple CPT-borehole combinations available across a wider area have been used and compared to calibrate a site-specific transformation model by fitting a Linear Regression line with the best fit.

3.2 SHANSEP FRAMEWORK

The SHANSEP framework (Ladd and Foott, 1974) is used to calculate the undrained shear strength of a soil at critical state. The framework calculates the undrained shear strength based on the effective stress of the soil, the degree of over-consolidation and two normalised parameters S_{nc} and m which need to be determined using laboratory testing:

$$s_u = \sigma'_v S_{nc} OCR^m \quad [13]$$

where S_{nc} is the normalised shear strength ratio under normally consolidated conditions, σ'_v is the vertical effective stress, OCR is the over-consolidation ratio (ratio of the past maximum σ'_v to the current σ'_v) and m is an exponent describing the strength increase with over-consolidation.

Once the S_{nc} and m parameters are established for a particular soil, the undrained shear strength can be calculated based on the stress history the soil exhibits in the field. Additional shear tests can optimise the normalised parameters S_{nc} and m, leading to greater accuracy in undrained shear strength predictions.

4 Reliability Analysis

Reliability analysis allows for uncertainty to be explicitly considered. Uncertain parameters include soil properties, the geometry of the slope and failure surface and the flood level. By accounting for uncertainties in analytical models as they arise, it is possible to obtain a probabilistic distribution describing the behaviour of an engineering system over all possible load ensembles.

Such a distribution allows one to consider the probability of the system in question failing and offers a much more meaningful insight into safety than a traditional deterministic factor of safety calculation (determined using unique estimates of the load and resistance). The performance function g(X) or limit state function of an engineered system is expressed as the difference between the system's capacity, C (resistance) and its demand, D (load), see Equation 14, this is closely linked to a systems factor of safety which is its capacity divided by its demand.

$$g(X) = (C - D)\begin{cases} > 0, \text{safe state} \\ = 0, \text{limit state} \\ < 0, \text{fail state} \end{cases} \quad [14]$$

$$g(X) = g(x_1, x_2, \dots, x_n) \text{for } i = 1 \text{ to } n$$

where X is a vector containing the different random variables (x_i) required to model the slopes safety. Safety is typically expressed either in terms of a reliability index, β, or a probability of failure, p_f. The probability of failure (p_f) is defined as the probability at which the performance function is less than zero, see Equation15.

$$P_f = P[g(X) \leq 0] \quad [15]$$

The reliability index (β) is defined as the number of standard deviations from the mean of the performance function to the design point (the point where capacity equals demand), Equation 16.

$$\beta = \frac{E[g(X)]}{\sigma[g(X)]} \quad [16]$$

4.1 System probability of failure

Slope instability is usually assessed independently of triggering mechanisms as it is not always obvious what will trigger a landslide. In this study, failure mechanisms have been analysed independently as well as systematically using an event tree to combine the individual failure probabilities by considering the chain of events necessary to trigger them, see Figure 1.

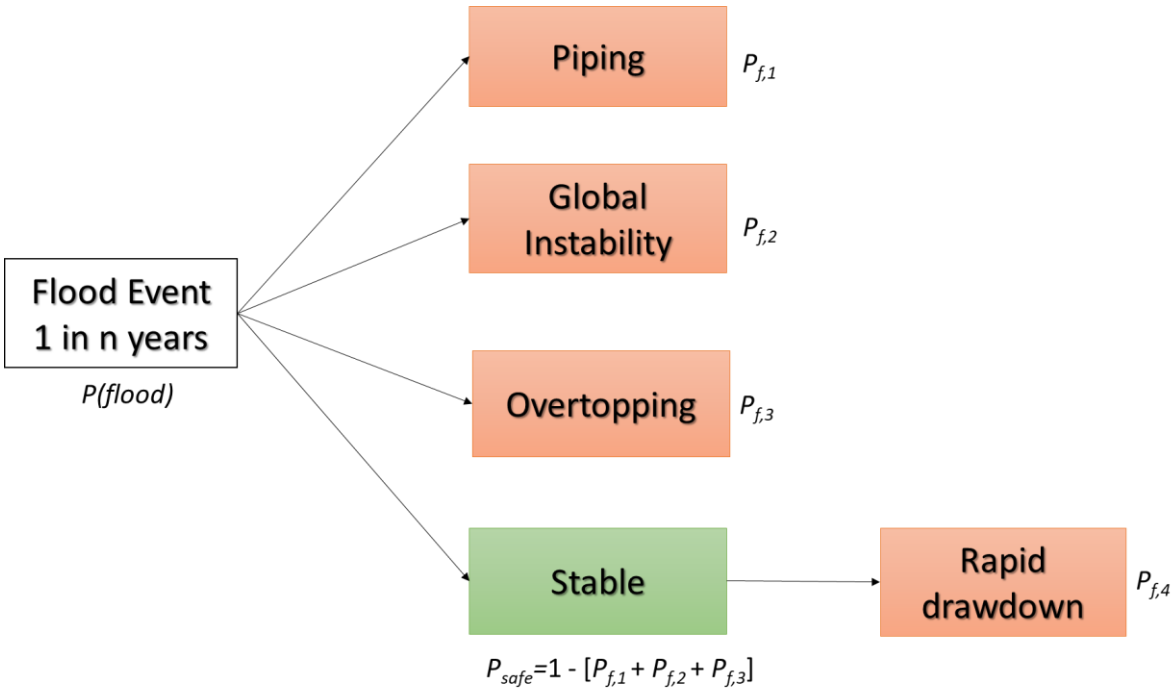

Figure 1 Event tree describing the different failure mechanisms possible and how they relate to one another

This framework assumes that the dyke can fail in one of four ways. Initially after a flooding event occurs the dyke can fail by piping, global instability or overtopping. If the dyke does not fail during the initial flood it may subsequently fail if the water level rapidly returns to normal following the event. Therefore, the true system probability of failure for dyke stability is as described in Equation 17. For this to occur however, a *1* in *n* year flood event must happen, the true probability of failure then must therefore consider the return period of the triggering event in this case flooding, see Equation 18.

$$p_{f,sys} = p_{f,1} + p_{f,2} + p_{f,3} + p_{safe}p_{f,4} \quad [17]$$

$$p_{hazard} = p_{flood}p_{f,sys} \quad [18]$$

4.2 Describing Geotechnical Uncertainty

Soil is a highly variable heterogeneous material whose structure and material properties can vary greatly across small distances (de Gast *et al.*, 2020). Some of this heterogeneity is due to the deposition and weathering processes the soil has undergone in its past, while some of may be caused by seasonal processes and human intervention. In order to calculate realistic reliabilities of geotechnical structures all variability must be accounted for.

Geotechnical uncertainty is not just limited to spatial variability, but is also complicated further by systematic errors in geotechnical laboratory and field tests, significant uncertainty in the physics underlying available predictive models and random testing errors. Typically, this uncertainty is split into two different categories; aleatory and epistemic uncertainty. Aleatory uncertainty is inherently fundamental to the material at hand such as the soils spatial variability (Reale, Xue and Gavin, 2017). Aleatory uncertainty cannot be reduced but can be measured and accounted if there is sufficient data through de-trending and statistical analysis. Epistemic uncertainty on the other hand is the result of a lack of knowledge and can be reduced through the accumulation of additional knowledge, this can be seen as model uncertainty and systematic error. Typically aleatory uncertainties govern data scatter whilst epistemic uncertainties cause a shift in the location of the mean trend i.e. either the model or the measured data is incorrect (Christian, Ladd and Baecher, 1994; Phoon and Kulhawy, 1999; Whitman, 2000), see Figure 2.

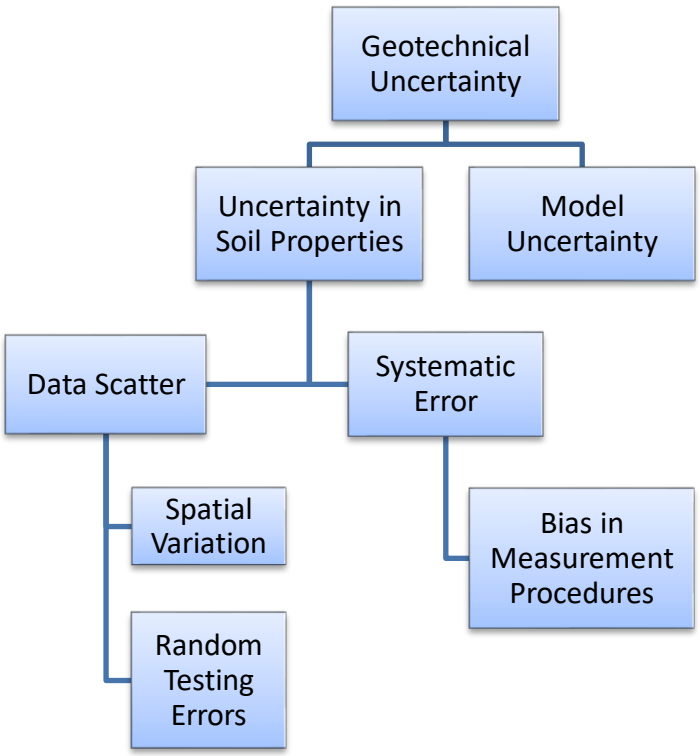

Figure 2 Disparate sources of uncertainty present in geotechnical reliability analysis

4.3 Uncertainty in Soil Properties

The interpretation of geotechnical parameters from site investigation data is a challenging task, particularly given that there is rarely sufficient data to accurately describe the ground conditions. This uncertainty can lead to under or overestimations of design parameters, and hence needs to be approximated using CPTs and laboratory tests from the area. As CPT measurements are continuous with depth, they are ideal for established the mean strength trend with depth and quantifying any variation about that plane (Prendergast, Reale and Gavin, 2017; De Gast, Vardon and Hicks, 2020).

Typically, to determine the uncertainty from a CPT trace the depth dependant mean trend is de-trended from the data leaving the variability behind. The variability can then be described using either a stochastic ground model that varies in time and space or more commonly using point statistics. Usually, data from all nearby CPTs are aggregated together for each layer, thereby minimising the impact of extreme values. Due to a lack of available information to correctly identify spatial variability this report will describe variability using point statistics i.e. a mean and a standard deviation for a layer. This overestimates variability, but is a conservative assumption.

4.4 Fragility Curve Generation

Fragility curves describe the conditional probability of reaching or exceeding a certain damage state when a hazard of a known intensity occurs (Martinović, Reale and Gavin, 2018; Rossi *et al.*, 2021). They can be used in combination with vulnerability assessments to comprehensively describe the risk profile at the site and provide a rational scalable basis for making risk-based remediation decisions. The fragility curves developed in this study will focus on Dyke failure should a flood of a certain magnitude occur, therefore they will take the following form.

$$p(f|h) = \text{Capacity}(h) - \text{Demand}(h) \quad [19]$$

where h describes the flood height.

4.5 Target Reliability

To deem a structure safe, it needs to meet certain predefined targets in terms of reliability index or probability of failure (Lacasse *et al.*, 2013; Reale, Xue and Gavin, 2017). These targets depend on a number of factors such as the potential consequences should a failure occur, the design life of the structure, socio- economic and political factors. If a structure is considered more important or of higher consequence, then it will need to meet a higher target reliability index to be acceptable than a corresponding structure of low significance. There is no commonly accepted failure rate in the geotechnical community for slope stability. (Santamarina, 1992) suggested that a failure rate of 0.0001 was acceptable for all slopes,

whereas within the same study a failure rate of 0.2 was considered adequate for slopes of negligible consequence, that require substantial investment to improve. There is also significant discrepancies between studies with Santamarina suggesting a failure rate of 0.01 was sufficient for large cuttings on a highway, which would be verging on an unsatisfactory classification from the U.S. Army Corps of Engineers (1999) guideline, see Table 1. (Christian, Ladd and Baecher, 1994) determined 0.001 to be a reasonable design value, assuming normally distributed variable, this aligns well with the target reliability index of 3.0 classified as an above average slope according by the U.S. Army Corps of Engineers.

Table 1 Suggested target reliabilities for geotechnical levees from the USACE

Expected performance level	Reliability index (β)	Probability of failure (P_f)
High	5.0	0.0000003
Good	4.0	0.00003
Above average	3.0	0.001
Below average	2.5	0.006
Poor	2.0	0.023
Unsatisfactory	1.5	0.07
Hazardous	1.0	0.16

5 Dutch case study - Oostmolendijk

5.1 Site Overview

The case study area “Oostmolendijk” is located between the towns of Ridderkerk and Hendrik-Ido-Ambacht, along the river Noord in the Zuid-Holland province of the Netherlands, see Figure 3 and Figure 4. The dyke, See Figure 1Figure 3 is a small part of the greater dyke ring IJssel-monde also known as Dike Ring 17, See Figure 4. Whilst the majority of the dyke ring is considered stable, the section considered here is affected by continuous ground settlement and cracking of the road surface resulting in ongoing maintenance problems.

Figure 3 Case study Site

Figure 4 Dyke Section 17-3, Oostmolendijk (in red), from Bossenbroek (2020)

Archive data shows that prior remedial work at Oostmolendijk between 1962 and 1968 proved to be very difficult with regular crack development and pore pressure variation resulting in large settlements, this in turn caused numerous delays in remediation. In 2013, a section of the dyke at Oostmolendijk was under repair when a global shear failure occurred within the dyke section. This was likely due to the underlying soft peat and clay layers being unable to support the additional weight added by the construction of a reinforced inner berm.

The predicted flood levels associated with key return periods for Oostmolendijk are shown in Table 2. This data is sourced from Hydra-NL a probabilistic model provided by the Dutch government which calculates the statistics of hydraulic loads specifically for the assessment of primary dykes in the Netherlands. An assessment of the stability of section 17-3 Bossenbroek (2020) suggests that Dike section is inadequate for a flood return period of 30,000 years.

Table 2 Flood levels associated with key return periods at Oostmolendijk

Return Period (years)	Flood Level (m+NAP)
10	2.750
30	2.918
100	3.087
300	3.215
1000	3.342
3000	3.432
10000	3.543
30000	3.658
100000	3.826

5.2 Dyke Geometry

The dyke geometry varies along the length of the section in question, see Figure 5. As this report is assesses the stability of the dyke using 2D cross sections it is necessary to divide the dyke into multiple sections which are presumed to be homogeneous for the purposes of analysis. The cross-sectional geometry for the different dyke sections were generated using the AHN viewer(*AHN Viewer*, 2020) which stores digital elevation data for the entirety of the Netherlands and is updated regularly. Oostmolendijk has a near uniform height profile along the length segment of interest with certain cross sections containing a small berm to provide extra stability.

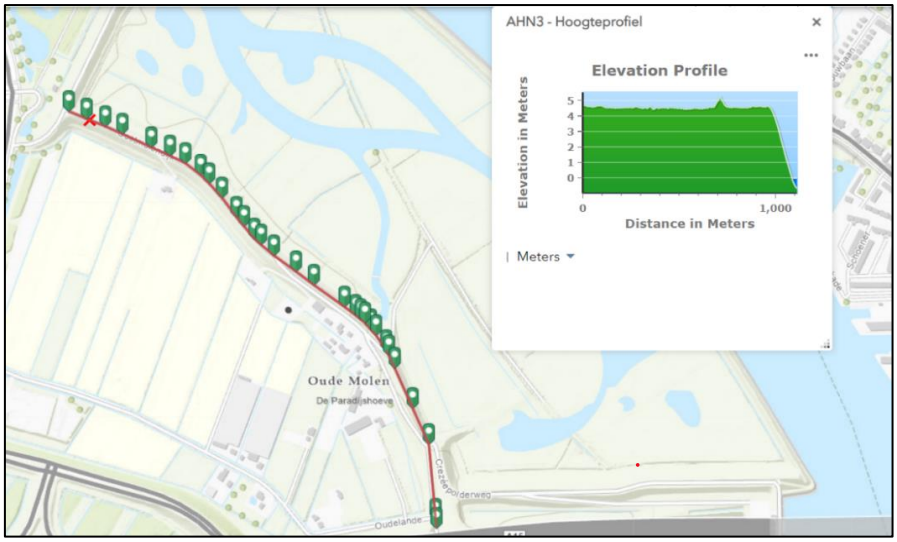

Figure 5 Dyke Segment along Oostmolendijk

The report demonstrates the assessment methodology with a focus on the particular dyke section shown in Figure 6 and Figure 7, which has had large localised movements with deep tension cracks developing in the landside slope. The dyke has a height of +4.7 m, NAP (Amsterdam Datum Level) at this point, and features a small drainage ditch after the slope finished on the field side. The river side is located to the right of the figure as seen in Figure 7. The analyses of additional sections are presented.

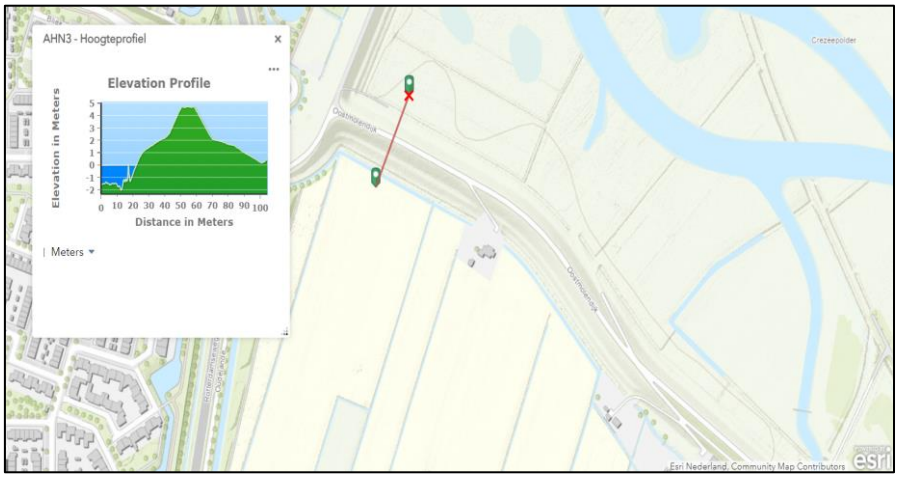

Figure 6 Dyke geometry for the Critical Section

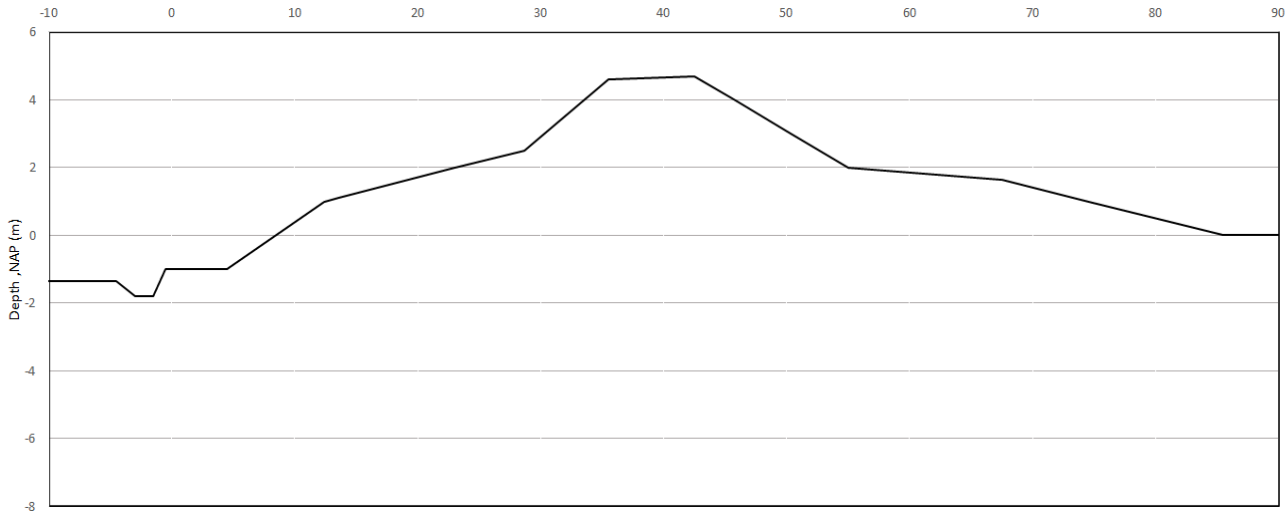

Figure 7 Dyke cross-section analysed herein

5.3 Geotechnical Interpretation

A detailed soil investigation covering a total length of 10.9 km of the dike section, including Oostmolendijk was available (Fugro 2020). This included CPT's, boreholes and laboratory tests carried out. Additional CPT and borehole data was extracted from Dinoloket (www.dinoloket.nl) whilst a site specific geophysical investigation was undertaken at the section analysed in this report by the University of Zagreb, See deliverable 3.1 of the Overflow project. The CPT profiles were used to estimate the stratification present in the subsoil as well to quantify the strength and variability of the material. While the geophysics and laboratory tests were used to determine the strength, stiffness and deformation characteristics of the material.

Depending on the material, different lab tests were used to measure the undrained strength, in clay the consolidated anisotropically undrained (CAU) triaxial test was used and in peat the direct simple shear (DSS) are adopted following Dutch practice. Additional in-situ tests such as the Torvane and pocket penetrometer were also performed in discrete locations primarily in the peat layer.

During testing some soil samples were consolidated beyond the maximum pre-consolidation pressure that the soil experienced in the field, to ensure that the soil was in a normally consolidated (NC) state before being tested to failure. This overloading of the sample is required when following the SHANSEP framework. Whilst other samples were consolidated to field stresses and subsequently tested, thus maintaining their original consolidation state. Oedometer tests were also performed on samples to determine the pre-consolidation stresses and Compression Index of the soil.

5.3.1 CPT and Soil Stratification Interpretation

CPT tests were carried out along the length of the embankment both at the dyke crest and in the adjacent field at regular intervals, see Figure 8. The CPTs show a uniform initial profile

predominantly consisting of Holocene era soft soil deposits to a depth of approximately 12 m below NAP overlying the Pleistocene era coarse sands, see Figure 9. As evident from the Dutch version of the Robertson Chart by (Robertson, 1990) classifications in Figure 10, there are three different soft soil layers present. An upper organic clay layer overlying a peat layer, which is in turn underlain by a lower clay. The exact depths and thicknesses of the layers vary across CPTs.

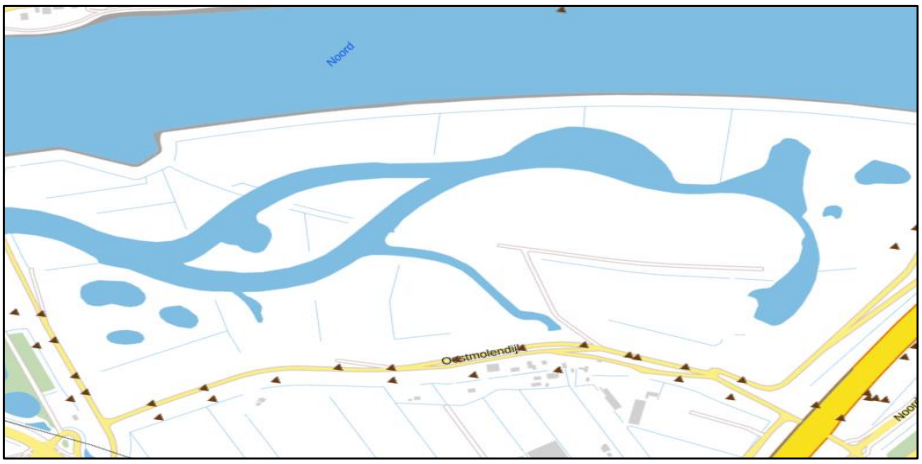

Figure 8 CPT locations at the test Site

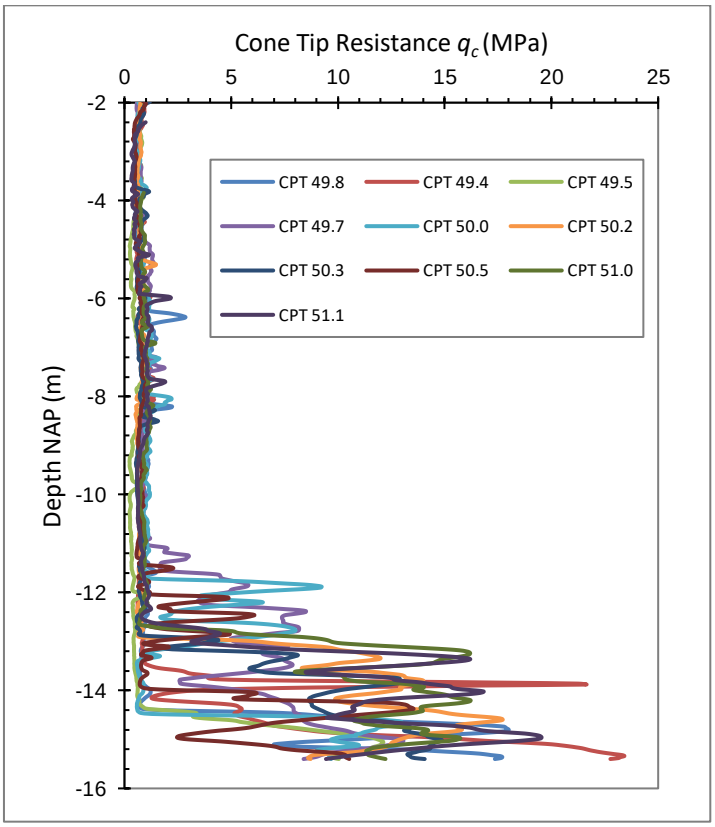

Figure 9 CPT traces at Oostmolendijk showing soft clay and peat layers extending to approximately 12m NAP

The dyke core is made of medium to fine sand, with a small percentage of silt capped with a clay cover to prevent water ingress and egress. It should be noted that no laboratory testing was carried out on the dyke material. Figure 10 shows the soil profile generated from a CPT including the cone end resistance, q_c, the ratio R_f (%) between the cone shaft friction and end resistance, that is used to identify the soil type and the interpretation of soil type using the Dutch version of the Robertson's soil classification chart.

Using the data gathered from the site investigation (Boreholes and CPTs) and available lithological and elevation maps of the wider area from Dinoloket, a detailed 2D soil stratigraphy was generated to describe the depth and extent of all soil layers underneath and surrounding the embankment, see Figure 11. The profile shows that the Peat layer thins considerably under the dyke suggesting post-construction settlement of more than 1m have occurred in this layer.

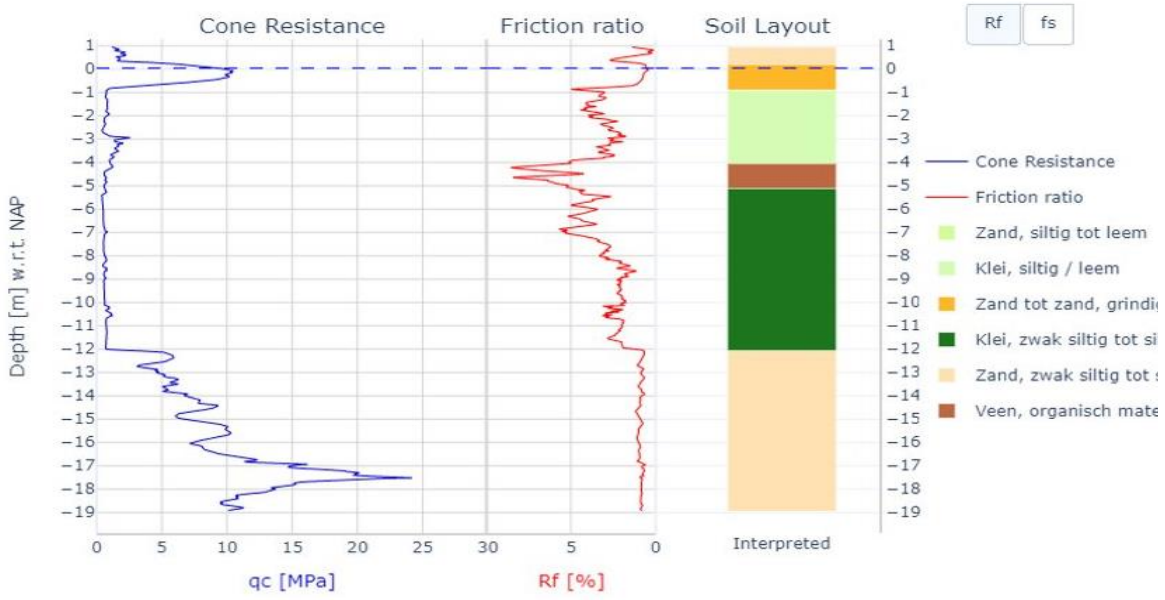

Figure 10 CPT soil classifications as per Dutch Robertson chart

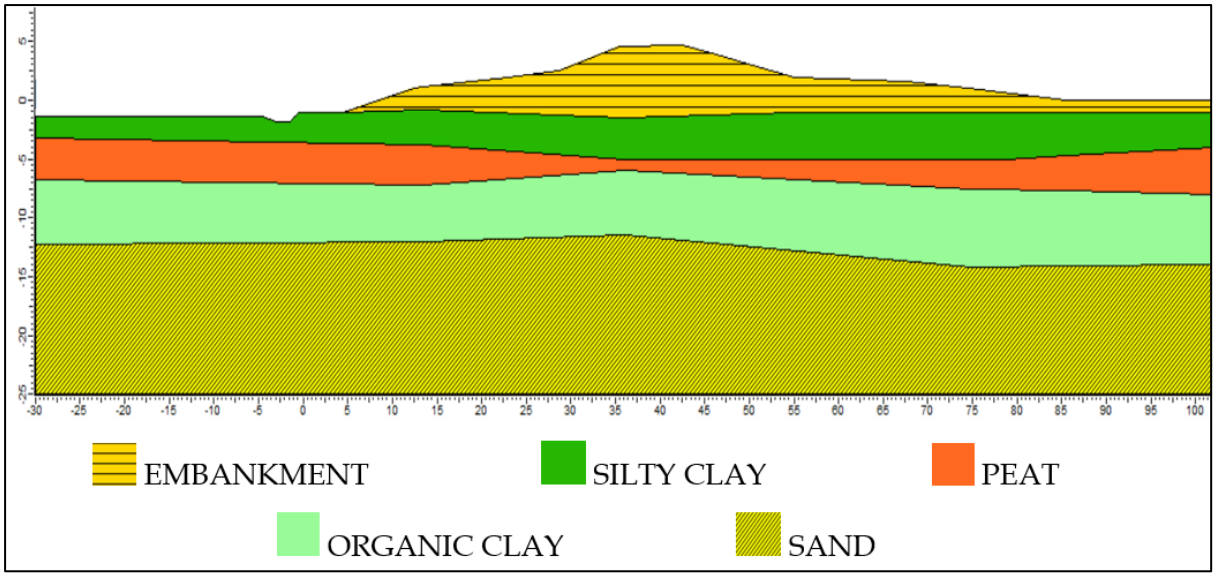

Figure 11 Interpreted soil stratigraphy

5.3.2 Geotechnical Parameters:SHANSEP

As described in section 3.2, to calibrate the SHANSEP model, three parameters are required. The first is the normally consolidated undrained shear strength parameter (S), the second, a stress exponent value (m) and lastly a measure of the over-consolidation ratio OCR. As the soft soil zone actually consisted of three layers, each soil layer was treated as an independent geological formation and the mean, variation and characteristic design values from the different layers are shown in Table 3. The OCR profile was determined using standard Oedometer and constant rate of strain, CRS tests in the laboratory and is shown in Figure 12.

Table 3 Point Statistics for Lab Measured SHANSEP parameters

Material	S, mean	m, mean	S, VC	m, VC	S, char	m, char
Upper Clay	0.29	0.89	0.15	0.02	0.25	0.87
Lower Clay	0.31	0.87	0.16	0.03	0.27	0.84
Peat	0.38	0.84	0.12	0.02	0.34	0.82

Laboratory measurements of undrained shear strength with depth from across Oostmolendijk are shown in Figure 13. Noting that triaxial tests were performed on clay samples with DSS tests on the peat samples, there appears to be more variation in strength

in the upper clay layer which becomes less significant with depth. If we ignore the outlier at -2m NAP we can see a gradually increasing undrained strength profile with depth.

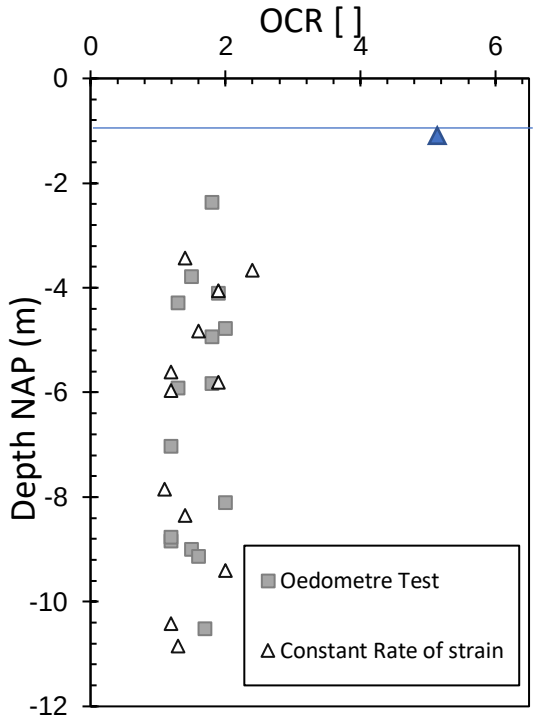

Figure 12 Comparison of Lab Measured and CPT Predicted OCR

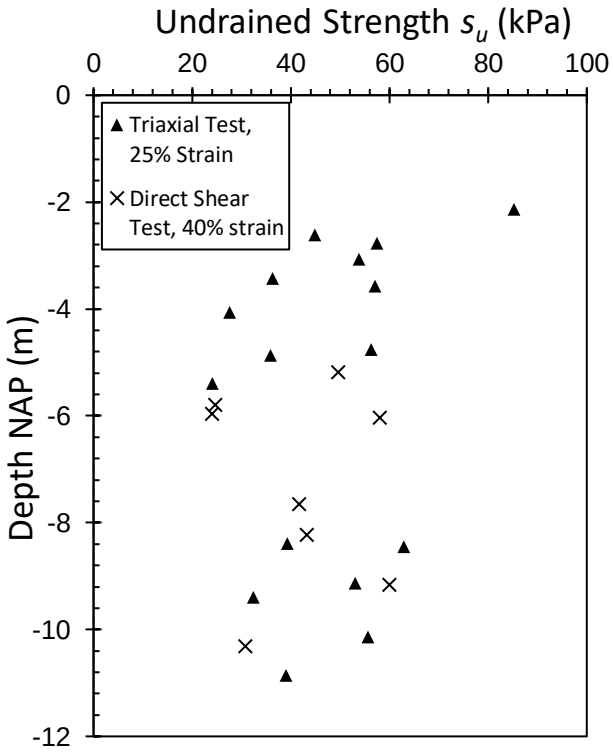

Figure 13 Measured s_u for various test at Critical State

5.3.2 Geotechnical Parameters: CPT method

The triaxial measured undrained strength values shown in Figure 13 were used to calibrate the site-specific transformation model for needed for the CPT based approach. The undrained strength values at 25% strain (Critical State) were compared with the net cone resistance of the nearest CPT at the same depth and the best fit line was established as in Figure 14 (a). Whereas in the peat layer direct simple shear results at 40% strain were used to calibrate the site-specific transformation model. This fit can be seen in Figure 14(b).

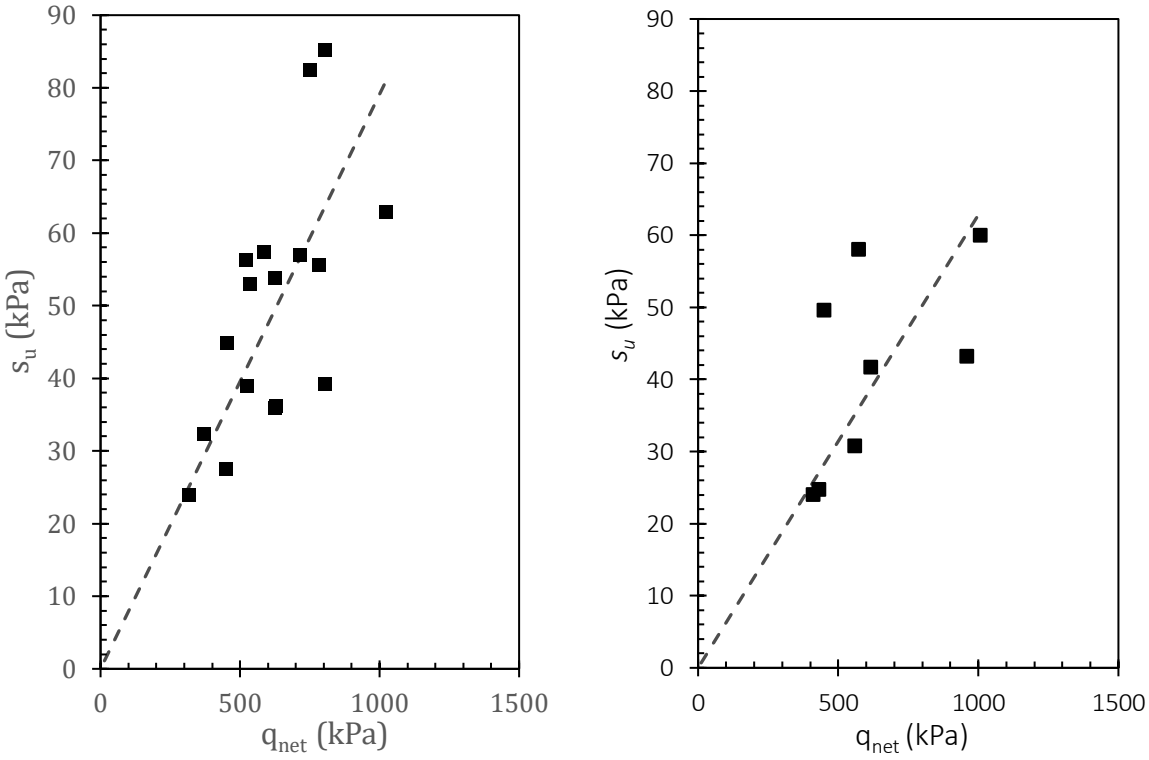

Figure 14 Site Specific Transformation Model Calibration for clay (a) and peat (b)

The relationship between the undrained shear strength and the cone tip resistance was determined using a linear regression model, where the slope of the fitted line is the N_{kt} value. N_{kt} values of 14 and 16 , see Figure 14, provided the best fit for the clay and peat layers respectively. An average N_{kt} of 15 describes the entire site satisfactorily, see Figure 15. Given that the exact depths and thicknesses of the peat and clay layers are unknown across the site and the small number of sample points, it seems prudent to adopt this average N_{kt} value for the entire site. This N_{kt} factor was then used to derive the undrained shear strength across the site using the CPTs as the input.

Table 4 Geotechnical parameters

MATERIAL NAME	UNSAT/SATURATED UNIT WEIGHT (kN/m³)	UNDRAINED STRENGTH s_u (kPa)	FRICTION ANGLE Φ	VARIATION COEFFICIENT
EMBANKMENT	18/20	$s_{u,top}$: 44 $s_{u,bottom}$: 41	0	0.30*
UPPER CLAY	14/16	$s_{u,top}$: 35 $s_{u,bottom}$: 30	0	0.32
PEAT	11/11	$s_{u,top}$: 32 $s_{u,bottom}$: 29	0	0.28
LOWER CLAY	16/18	$s_{u,top}$: 30 $s_{u,bottom}$: 33	0	0.25
SAND	20	-	35	0.23*

*Variation coefficients as given in Geotechnical Investigation report (Fugro 2020).

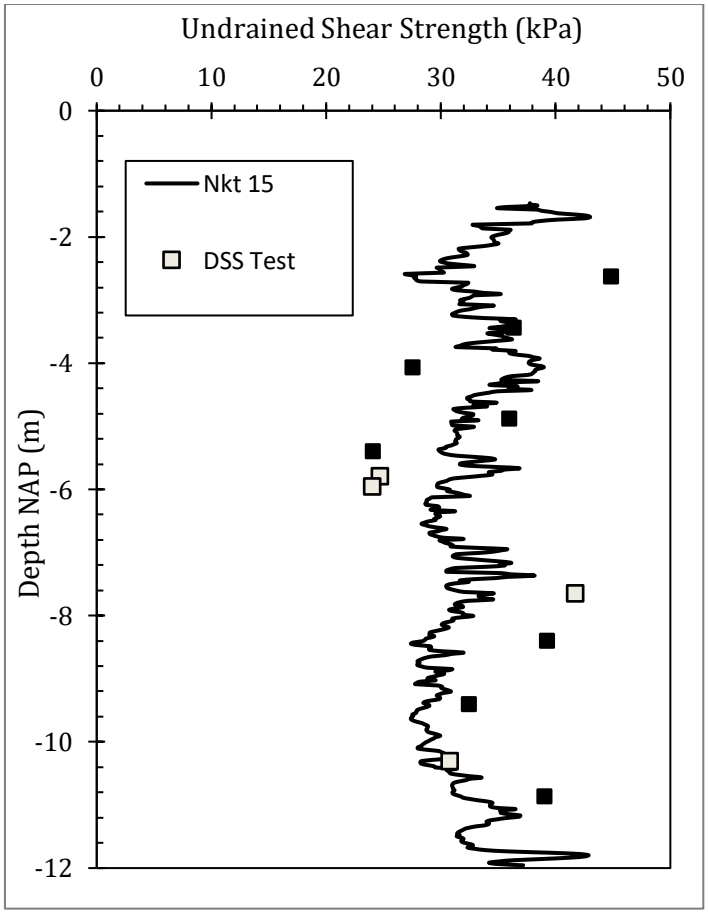

Figure 15 Comparison of Undrained Strength for different Nkt Values

5.3.3 Comparing Undrained Shear Strength Methods

The undrained shear strength profile was calculated using the SHANSEP formula using the mean and the characteristic values of 'S' and 'm' as mentioned in Table 3 and the measured OCR values. The SHANSEP strength profile is compared to the CPT derived undrained strength profile (using an N_{kt} of 15) and the measured laboratory shear strength data, see Figure 16.

The CPT derived strength profile closely matches the laboratory test data. The SHANSEP derived profile starts as a lower bound fit in the upper clay layer, but becomes less conservative with depth. Eventually becoming non-conservative in the lower clay layer. Examining Figure 16, one can see that the SHANSEP characteristic design profile is very close to the mean SHANSEP design profile. Given that the COVs measured at the site are quite large varying between 0.2 and0.32, one would expect a much larger difference between the mean and characteristic design profiles. The SHANSEP model just considers variability at critical state, where soils are at constant volume and at their least variable. This is not the representative state of the in-situ soil and doing any statistics on this soil is likely to underestimate the true variability. In particular, the SHANSEP approach removes any variability related to the stress history of the deposit. Variability in the SHANSEP approach is determined using a small number of tests which again makes true variability hard to determine. By definition, a characteristic design value should be conservative, otherwise it simply masks true soil behaviour, while providing the appearance of conservatism. A fully probabilistic approach using a mean fit and measured in-situ variability, such as the CPT based approach, would be more prudent when evaluating high risk sites.

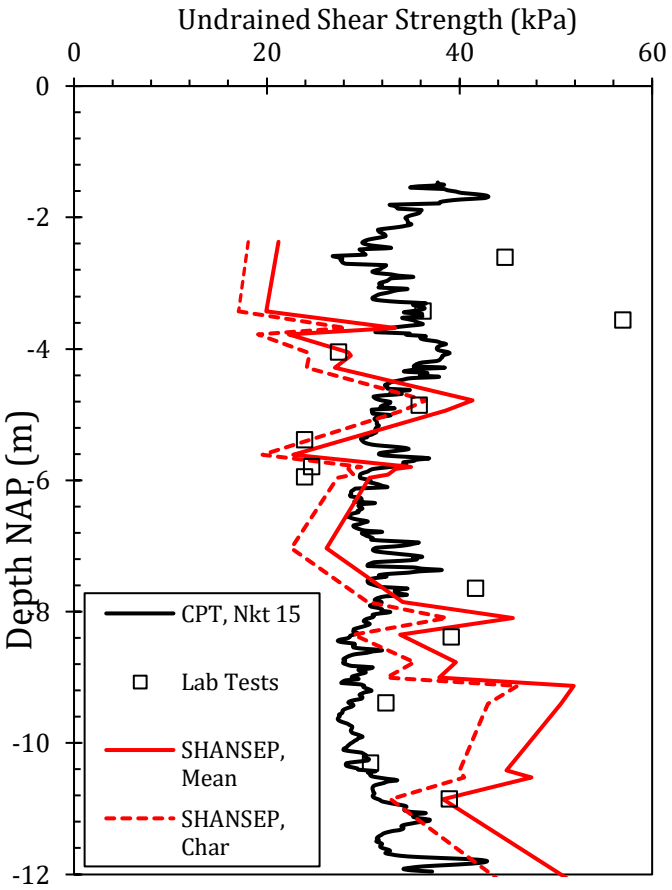

Figure 16 Comparison of Undrained Strength using a) SHANSEP, b) CPT-based Method and c) Lab Test

5.3 Fragility Curves

5.3.1 Piping Fragility Curves

Using the limit state described in section 2.4 and the probabilistic framework outlined in section 3, fragility curves were developed to assess the likelihood of piping failure given the occurrence of a flooding event. The unit weight and permeability of soil were considered as probabilistic variables. Typically in-situ permeability has a large, coefficient of variance, COV (Phoon and Kulhawy, 1999) across a site as the presence of any cobbles, boulders, air cavities, vegetation, burrows, cracks etc. will significantly alter infiltration, flow path and rate. In this study a mean sand permeability value of 2×10^{-5} m/s was assumed, while four different COVs were considered {0.1, 0.2, 0.3 and 0.4}. Figure 17 shows the results of this analysis, while Figure 18 shows the same results plotted on a log scale. From Figure 17 it appears there is little difference in the probability of failure as the flood level reaches approximately 3.5m. However from Figure 18 it can be seen that at much lower flood levels there is a significant spread in the results. Ultimately if we consider a target probability of failure of 0.001 (10^{-3}) it is necessary to consider the variations shown in the log plot. At a COV of 0.4, a 1 in 10 year

flood event of 2.75m, would have a probability of instigating a piping failure of 7 x 10^{-3}, while at a COV of 0.1 the probability is almost two orders of magnitude lower at 6 x 10^{-5}. In general piping failure does not appear to be significant for flood events lower than the 1 in 1000 year event (3.342m), but beyond this point it quickly becomes the dominant failure mechanism at higher COVs.

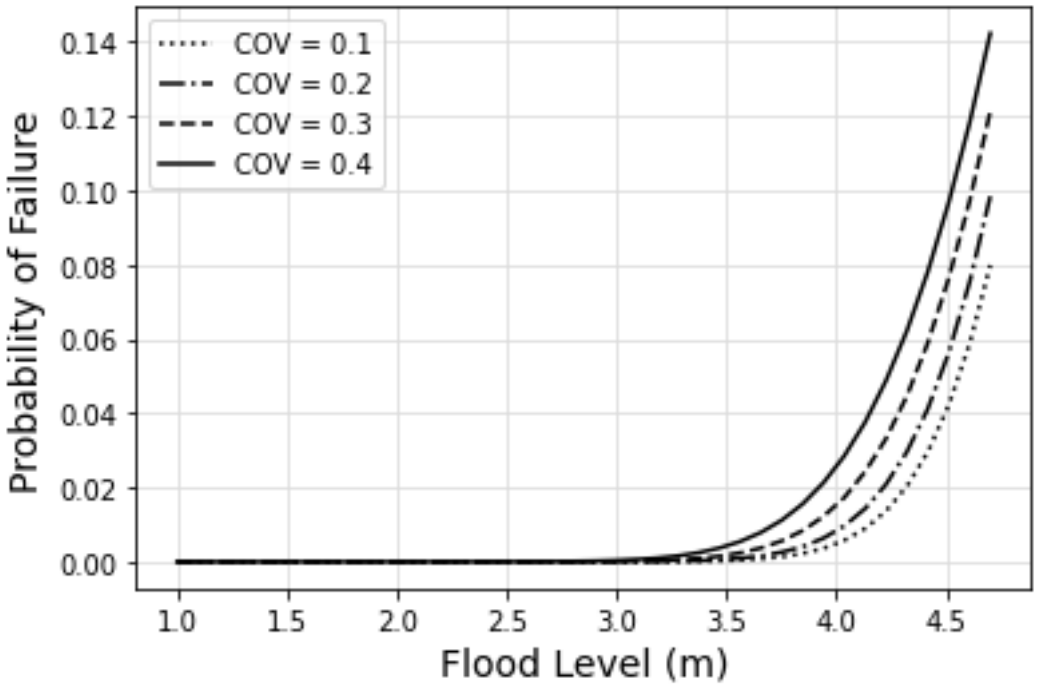

Figure 17 Fragility curve showing the effect of increasing the coefficient of variation of the soil permeability.

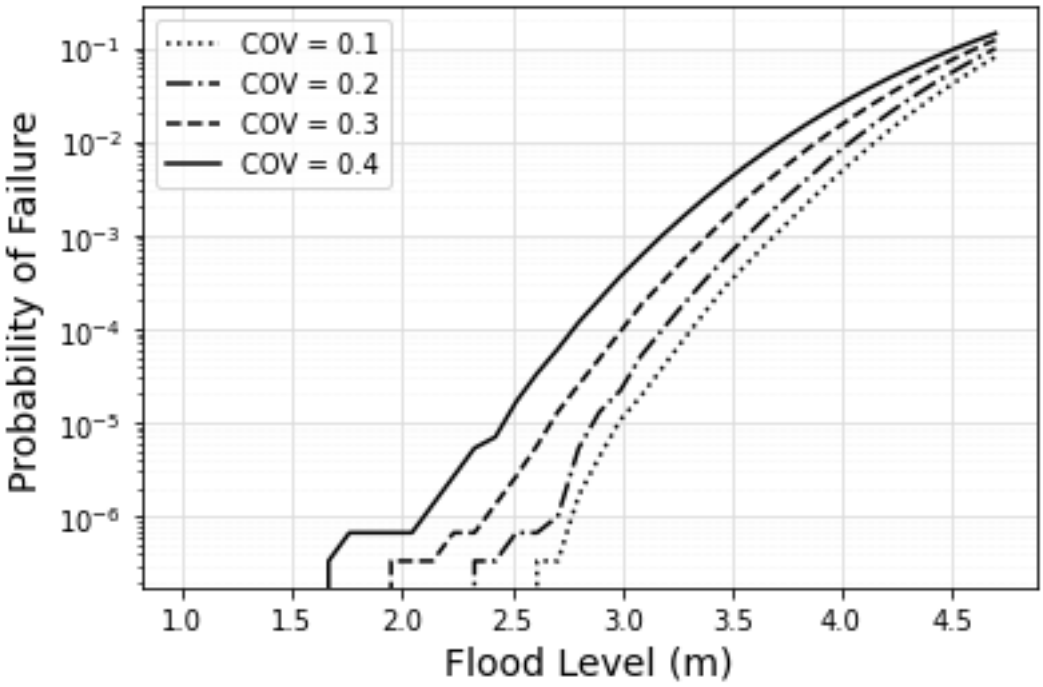

Figure 18 Logplot of Figure 18 showing more clearly the change in likelihood as the flood level increases

As the exact permeability on site is unknown a value of 2 x 10^{-5} m/s was assumed based on a literature study. A sensitivity study was carried out to investigate the impact changing the mean soil permeability value has on results. Figure 19 and Figure 20 (log-scale) show how sensitive the dyke is to movement in the value of the mean permeability, if for instance the sand layer was to contain slightly more silt reducing the permeability to 1 x10^{-6} . In this case piping ceases to be a likely failure mechanism under any of the possible flood conditions. If on the other hand the permeability of the soil is underestimated by a small degree, the probability of failure is much greater. For example, if the permeability was 4 x 10^{-5} m/s then a 1 in 10 year flood event would have a 1% chance of causing the dyke to fail. To ensure stability of the dyke system extensive permeability tests should be carried out across the site to quantify the expected distribution of permeability.

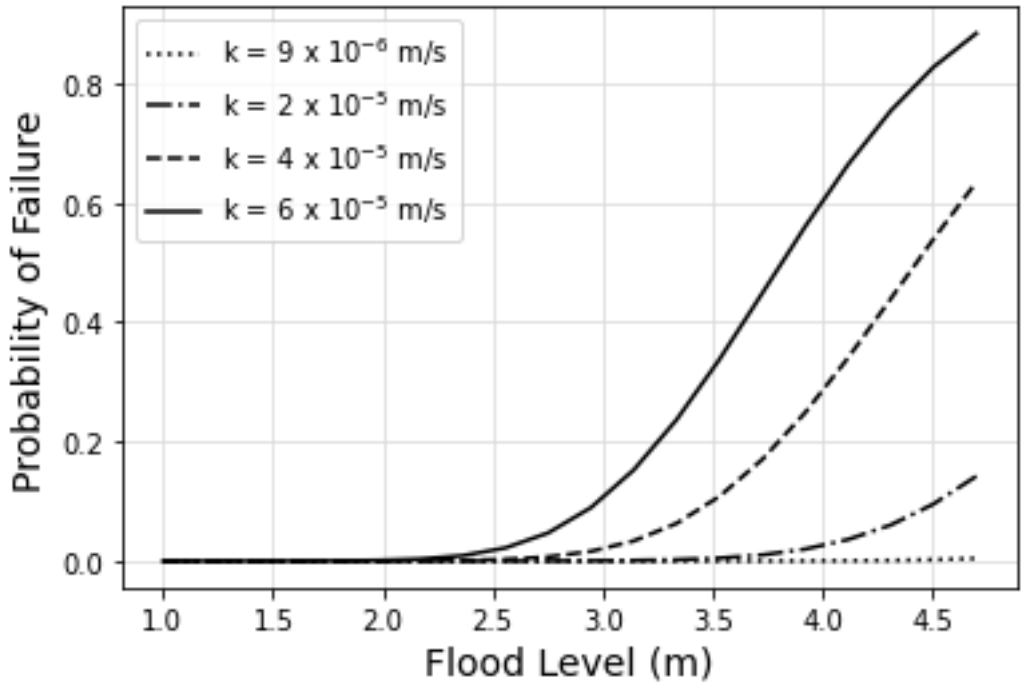

Figure 19 The effect of changing the mean permeability on probability of failure

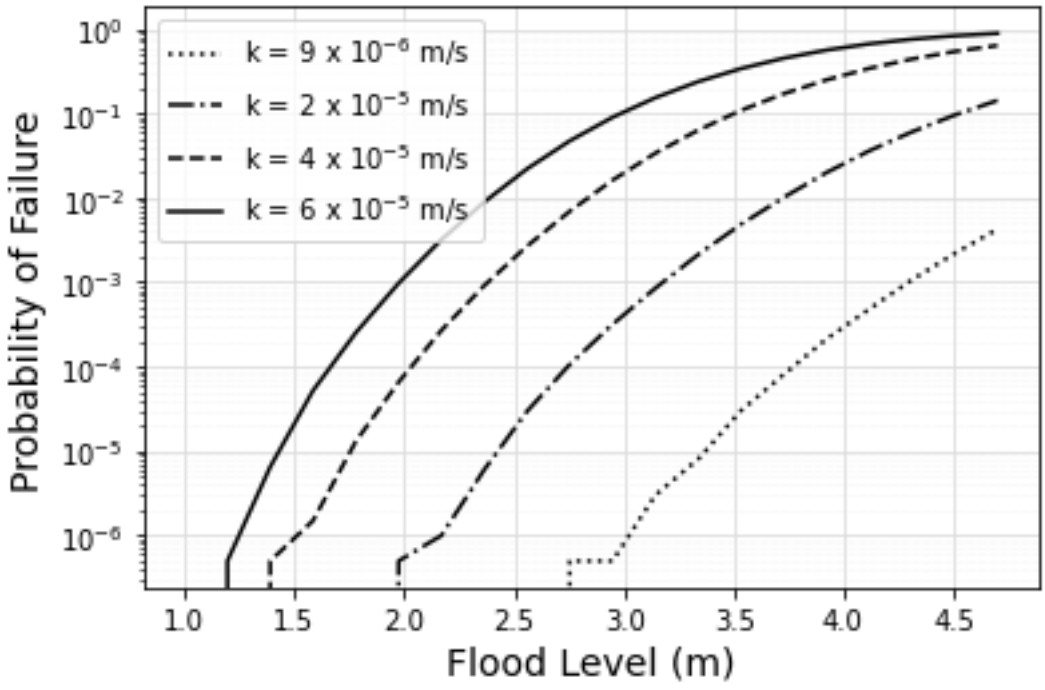

Figure 20 Log- scale fragility curve showing the how sensitive the dyke is to changing permeability values

5.3.2 Global Instability and Overtopping Fragility Curve

A combined fragility curve for global stability and overtopping was generated using the methodology from sections 2,3 and 4 using the geometry and geotechnical interpretation and parameter variation outlined in section 5. The results are shown in Figure 21. When the flood height exceeds the height of the dyke, additional shear stress caused by overtopping are included in the analyses. It should be noted that overtopping is extremely unlikely to occur at Oostmolendijk, Table 2 shows that a 1 in 100,000 year flood level isn't high enough to overtop the dyke, rendering such calculations unnecessary. The calculation is included herein merely for illustrative purposes. Examining the more likely 1 in 100 year event, which returns a flood height slightly over 3m it can be seen from Figure 21 that this causes a probability of failure just below 1%. Considering the global failure mechanism in isolation, Oostmolendijk would classify in the condition *below average slope* on the USACE target reliability criteria verging on poor, see Table 1. This classification is only marginally improved for a 1 in 10 year flood event and as such the safety provided by the dyke during flood events should be considered questionable. Overall global instability has proved to be the most significant failure mechanism at Oostmolendijk and even if ultimate failure does not occur the lack of safety margin in the system is likely to cause serviceability failures leading to large ongoing settlements.

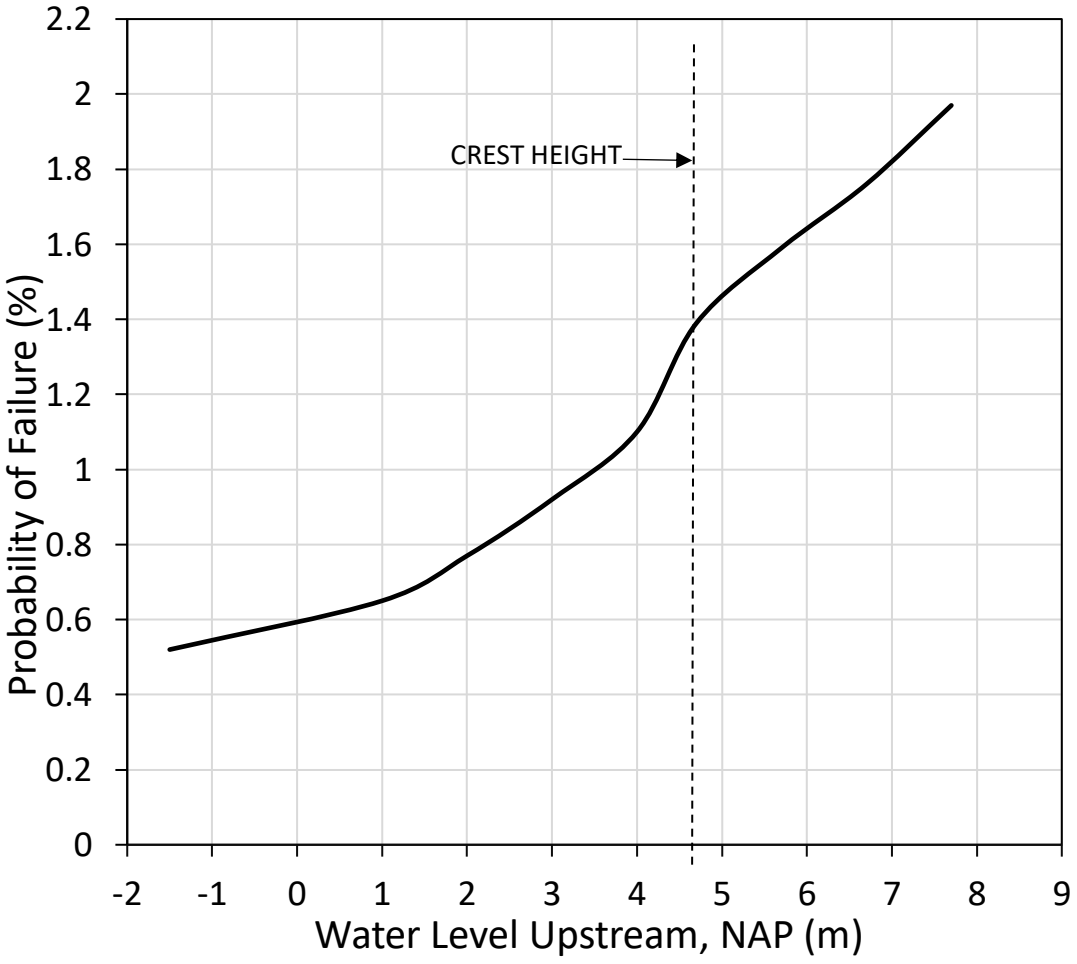

Figure 21 Fragility curve showing the change in global stability as flood level changes

5.3.3 Rapid Drawdown Fragility Curve

The final failure mechanism considered is the likelihood of the Oostmolendijk failing during a rapid drawdown event as the river returns to its normal level following a major flood event. Figure 22 shows the results of this analysis. The curves start (in the left-hand side) at the highest water level for the given flood event(e.g. 3.342 m for a 1:1000 year flood). The probability of failure is dependent upon the total change in head height with the likelihood of failure increasing as the drawdown level increases (i.e. the water level drops on the river side). The 1 in 10, 1 in 100 and 1 in 100 year drawdown events all have a probability of failure between 0.06 and 0.07, giving a reliability index of approximately 1.5, see Table 1. Figure 22

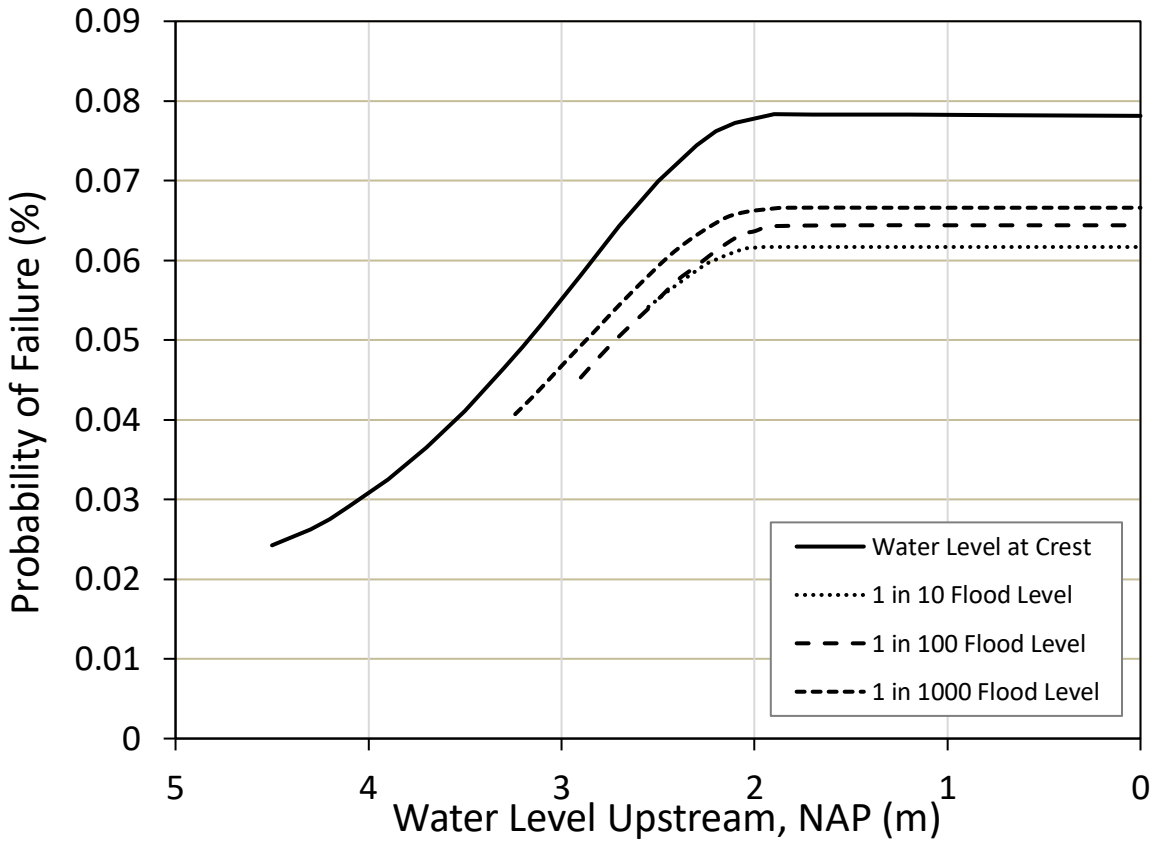

Figure 22 Fragility curve showing the change in stability following rapid drawdown

5.3.4 System probability of failure curve

Using Equation 17 derived from the event tree outlined in Figure 1, the results from the piping, global stability and rapid drawdown failure mechanisms were combined to produce a fragility curve which describes the system probability of failure, see Figure 23. This curve is dominated by the global stability fragility curve until the flood level surpasses 3 m, at which point the piping mechanism becomes the dominant failure mechanism. A 1 in 100 year flood event has a probability of failure of 1%, which means the dyke condition is significantly below

average verging on poor using the USACE rating system, see Table 1. This curve does not take flood return periods into account and as a result the true probability will be lower. However even without a flood event Oostmolendijk has below average reliability driven by the low undrained shear strength in its bearing layers.

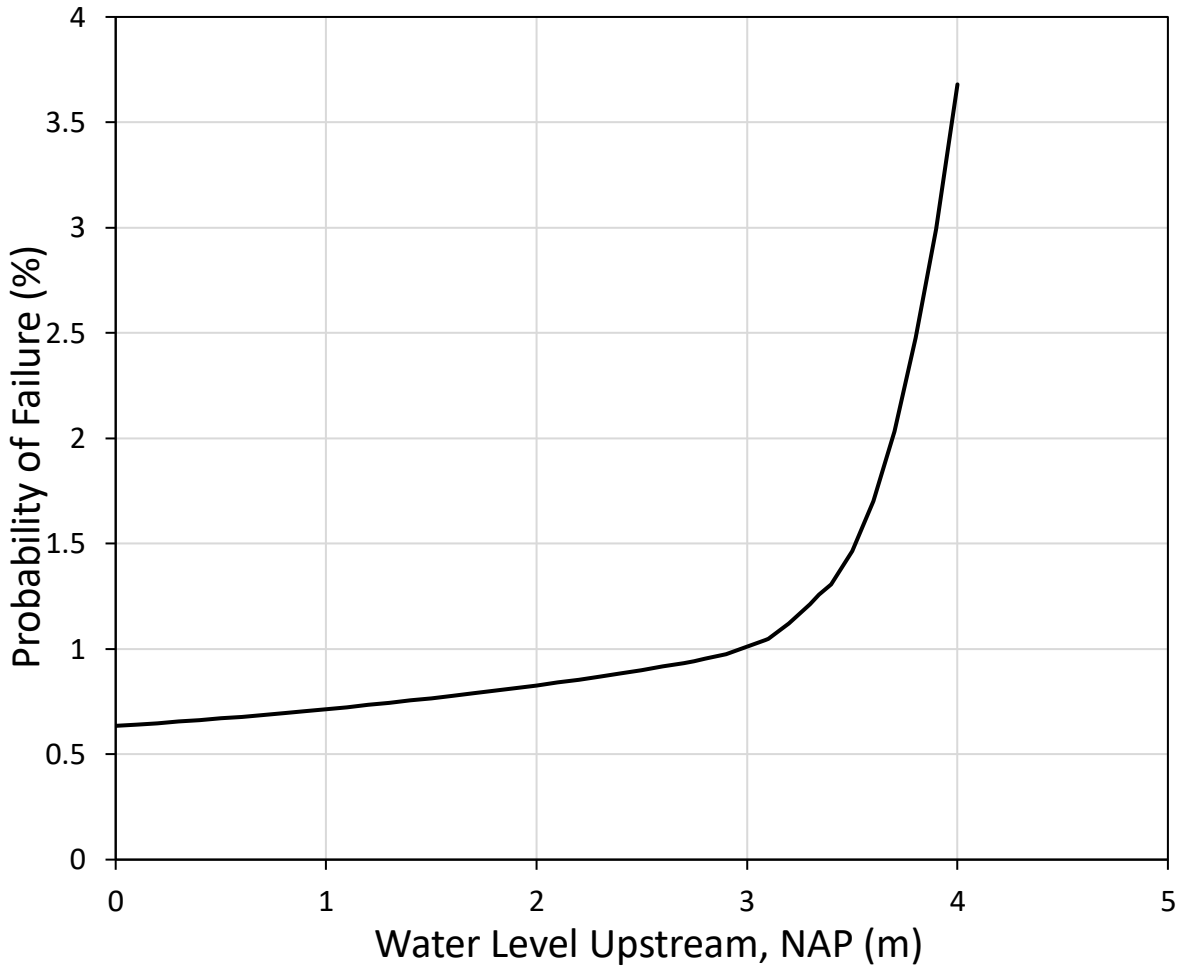

Figure 23 Combined system probability of failure curve

5.4 Consider of other cross-sections at Oostmolendijk

Whilst the height of the dyke at Oostmolendijk is relatively constant along its length, the dyke body varies in thickness at several key sections due to the presence of berms and road intersections. To capture the changing geometry of Oostmolendijk, four different sections were taken at discrete locations along the kilometre-long dyke. The locations selected can be seen in Figure 24. The geometries for these sections were obtained using the AHN viewer and are shown in Figure 25. These sections have been analysed and used to produce fragility curves that describe the probability of dyke failure (considering macro instability, piping, overtopping and rapid drawdown) should a flood event occur. A system probability of failure curve is used to combine the different failure mechanisms into one fragility curve.

Figure 24 Location of the selected sections

The dyke sections are labelled from 1 to 4 moving from left to right as shown in Figure 24. Dyke section 1 consists of a 4.7 m high crest with initial steep slopes on either sides before transitioning to more gradual berms at 3 m above ground level, see Figure 25. There is a small ditch on the field side which causes a sharp change in berm angle near ground level. Dyke section 2 is slightly shorter at 4.65 metres and has a very similar shape to section 1 except for a steeper transition from the berm to the dyke on the field side. Section 3 has a 5.1m high crest with a wide berm supporting the dyke approximately at 3m NAP on the field side, which very gradually transitions to field level. The riverside does not have a berm. Finally, section 4 is approximately 4.6 m tall with a wide berm at 2 m NAP on the field side, which steeply transitions into a small ditch, the riverside does not have a berm, but the floodplain is higher here at approx. 1.5 m NAP, i.e. 1.5 m higher than the surrounding sections.

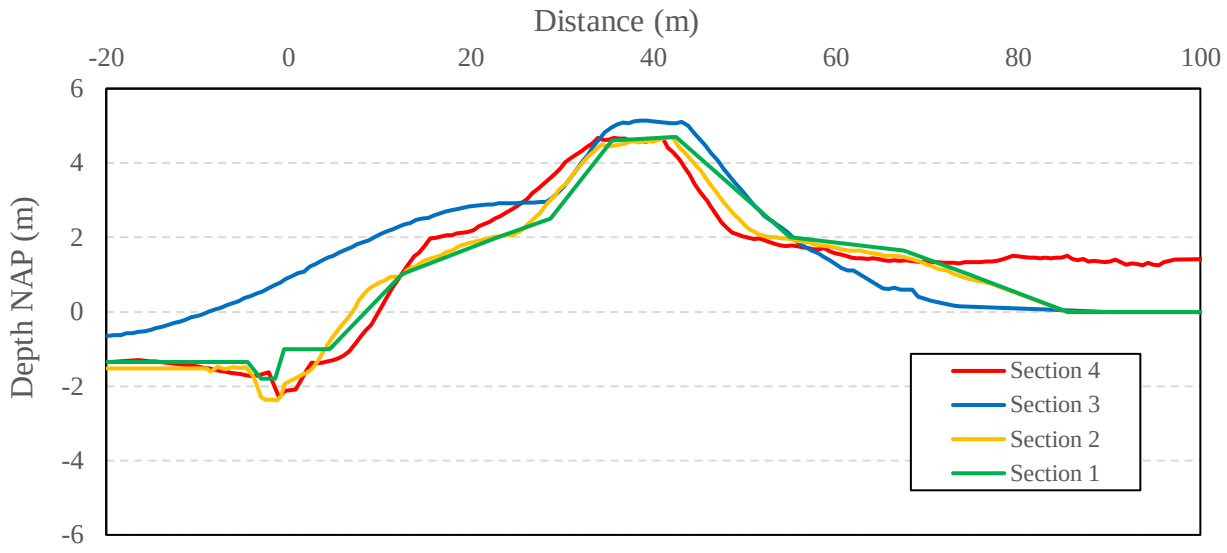

Figure 25 Profile geometry for the Oostmolendijk sections

The most likely global failure surface for all sections occurs along the boundary of the second clay layer and the deep sand deposit, See Figure 26. The second most likely failure surface is along the interface of the peat layer and the underlying clay. The factors of safety vary from a low of 1.59 (section 4) to a high of 2.1 (section 3). The difference in safety between sections is driven by the width and angle of the berm on the field side. The sections with a very wide (>40m) gradual berm such as section 3, have a very long failure surface and consequently have a lot of material resisting failure. In comparison, section 4 has a berm which steeply transitions to field level, this sharp transition means that there is less material to the left of the centre of rotation to resist failure which makes failure more likely.

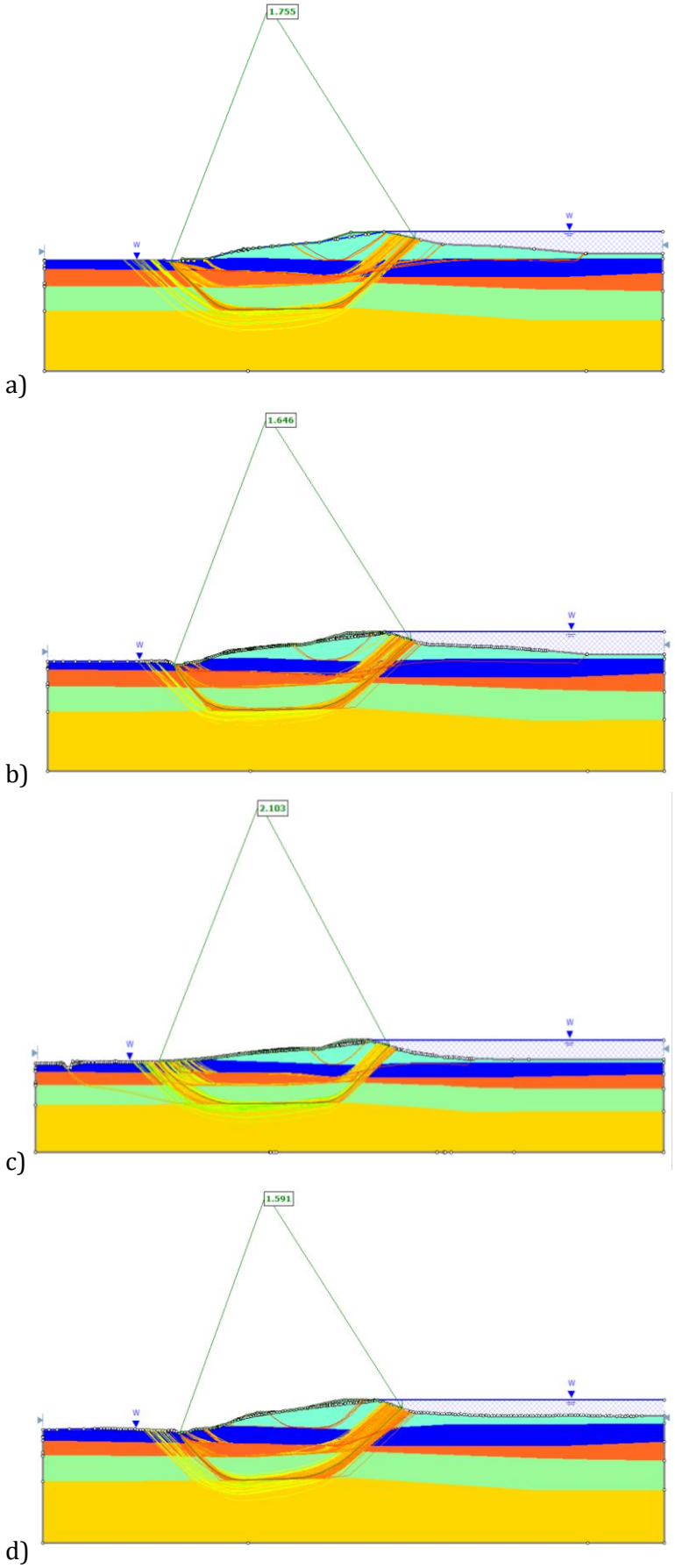

Figure 26 Global failure surfaces for sections 1-4 at maximum flood level are shown in a) to d) respectively

The likelihood of a flood event inducing a macro failure i.e. a large rotational failure, gradually increases for all sections as the flood level increases, see Figure 27. For sections 1,2 and 4, the rate of change of the probability of failure with flood height increases for flood levels in excess of 3.8m. This trend is not seen in section 3 due to the presence of an extremely wide berm on the field side of the problem. The probability of failure at the sections from a 1 in 100 year flood event are 0.9, 1.8, 0.2 and 2.4% respectively. This would classify section 4 as poor on the USACE levee rating scale and would classify sections 1 and 2 as below average. Section 3 on the other hand would be classified as above average.

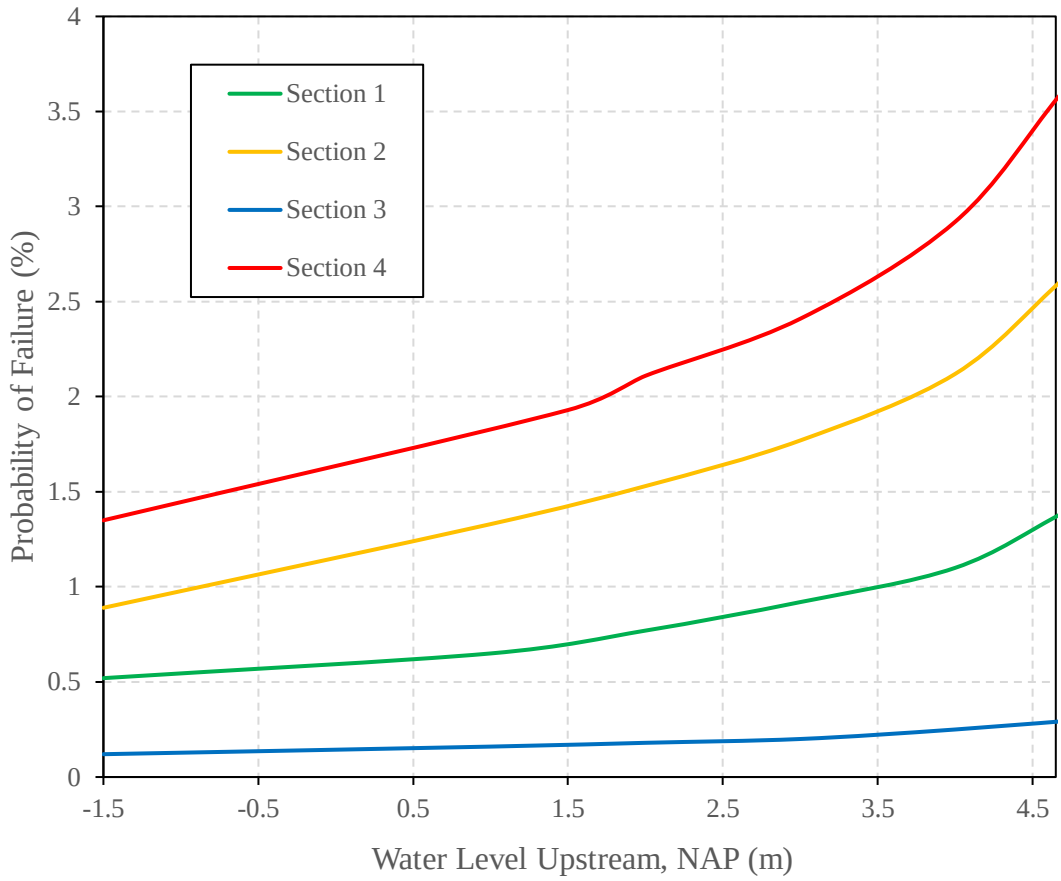

Figure 27 Macro-instability fragility curves for all sections

The system probability curves shown in Figure 28 accounts for all the failure mechanisms combined. Initially the macro instability mechanism dominates the system curves however as water levels increase all the failure mechanisms individually increase in likelihood causing a rapid increase in system probability of failure when flood waters exceed 3 m NAP. At water levels in excess of 3m NAP, piping becomes the dominant failure mechanism. The probability of failure of the individual sections from a 1 in 100 year flood event are 1.0, 1.9, 0.33 and 2.5% respectively. This would classify section 4 as poor verging on unsatisfactory on the USACE levee rating scale and would classify sections 1 and 2 as below average to poor. While section 3 would be classified as average.

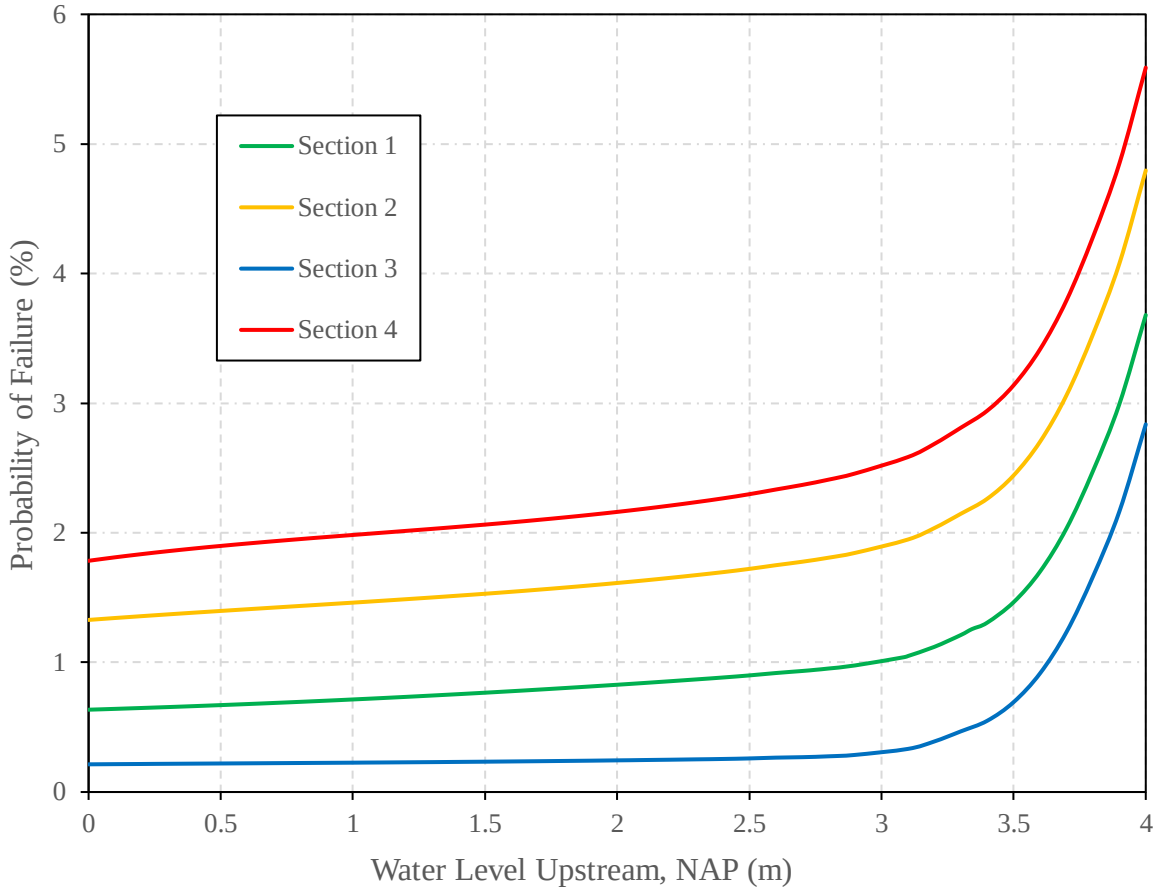

Figure 28 System probability of failure fragility curve for all sections

6 Croatian case study – riverbanks in Karlovac

6.3.1 Site Overview

The city of Karlovac is situated in the central continental part of Croatia at the meeting point of the lowland and mountainous regions, between Slovenia to the west and Bosnia and Hercegovina to the east. It is located at the intersection of important road and railway routes from Zagreb to Rijeka and Split and therefore has an important role in transport and the economy of the country Karlovac is also situated at the intersection of four rivers, Kupa, Korana, Dobra and Mrežnica, making it extremely prone to flooding. Many settlements, city districts, local roads and the state road D36 are regularly flooded with floods, also threatening important international and regional rail lines. In the flood prone area of Karlovac there are a total 375 cultural heritage sites and cultural object, amongst which is the renaissance fortification system called 'Karlovac Star'.

Within the oVERFLOw project, the assets analysed include 1.5 km of riverbanks on each side of river Kupa, in the city centre, Figure 29. Between the selected riverbanks, two case study bridges are located and their vulnerability analysis is covered by the another Deliverable (Kosič et al., 2022). The riverbanks are mostly up to 10 m high, however with variable geometry and slope angle. At some parts, a stone wall is located on the top of the riverbanks, serving as an additional protection during high water event. However, this wall is generally in poor condition with many washed-out joints. On last 100 meters of the left side and 50 meters of the right side there is an embankment resting on the top of the riverbanks. These embankments represent the continuation of the riverbanks and as such form an integral part of city center flood protection system.

Figure 29 Riverbanks in the city centre along the Kupa river

6.3.2 Selection of the relevant cross sections for analysis

As elaborated in the Deliverable 3.1 (Bačić and Kovačević, 2021), which deals with the investigation works and monitoring of embankments and riverbanks, aerial photogrammetry of the case study was followed by the generation of a detailed 3D point cloud. This provided automatic extraction of relevant (characteristic) cross sections, assisted by the enhanced algorithm to ease and speed the procedure. Therefore, based on the variations in the overall geometry, riverbank characteristic zones are identified. Having the results of investigation works in every zone (Bačić and Kovačević, 2021), provided the basis for vulnerability analysis, i.e. development of riverbank fragility curves. The location of each identified zone is shown in Tables 5 and 6, and on Figure 30.

Table 5: Selected zones of the right riverbank

Right riverbank			Total length of zone (m)
Number	**Designation**	**Chainage (*from* km - *to* km)**	
1	D1	0.000 - 1.000	1175
		1.200 - 1.375	
2	D2	1.000 - 1.200	200
3	D3	1.375 - 1.525	150
4	D4	1.525 - 1.550	25
		Total length (m)	**1550**

Table 6: Selected zones of the left riverbank

Left riverbank			Total length of zone (m)
Number	**Designation**	**Chainage (*from* km - *to* km)**	
1	L1	0.000 - 0.075	955
		0.175 - 0.400	
		0.470 - 1.125	
2	L2	0.075 - 0.175	245
		0.400 - 0.470	
		1.125 - 1.200	
3	L3	1.200 - 1.375	175
4	L4	1.375 - 1.550	175
		Total length (m)	**1550**

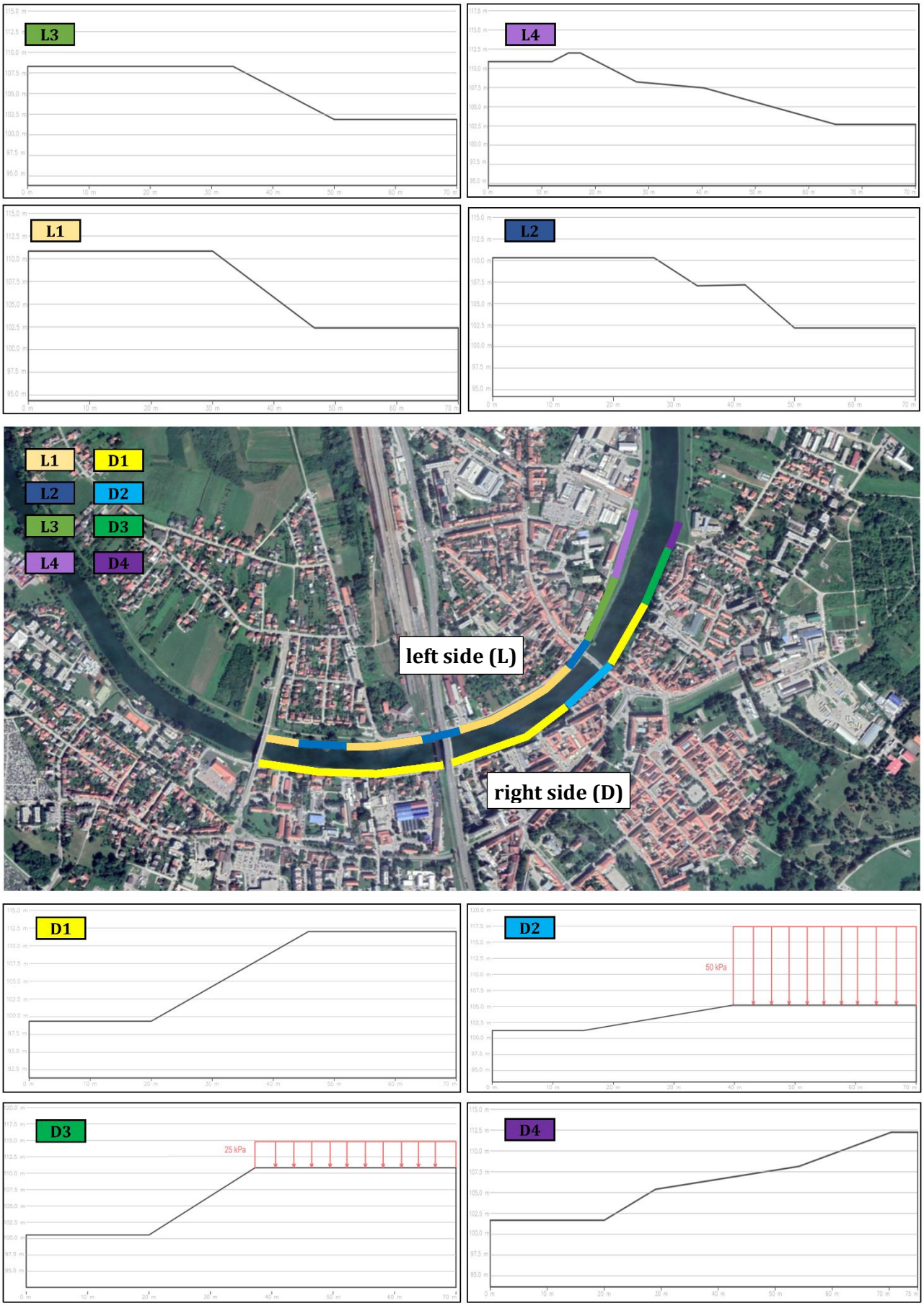

Figure 30 Location of identified riverbank zones based on their geometry

6.3.3 Selection of the soil parameters

To determine the riverbank subsoil conditions for vulnerability analysis, as well the variability of key soil parameters, several investigation methods were considered, with the detailed elaboration on investigation methods given in deliverable 3.1 (Bačić and Kovačević, 2021). These included soil drilling with soil sampling and laboratory testing and CPTU testing. In addition, geophysical investigations of electrical tomography (ERT) and multichannel analysis of surface waves (MASW) were used to supplement the knowledge of geological-structural characteristics of the riverbanks. The characteristic soil layering is shown on Figure 31. The soil layering was consistent along the riverbank and it included the low plasticity clays in upper 5 to 6 meters, overlying the clayey sand layer to larger depths.

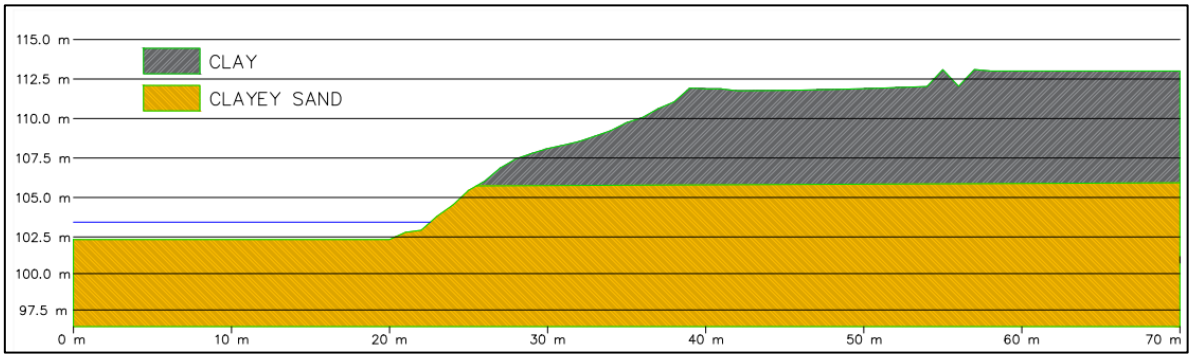

Figure 31 Characteristic cross section of a riverbank layering

While the laboratory testing (Figure 32 as an example of one of DSS tests) was used to determine the drained strength characteristics of the upper clay layer, the lower clayey sand layer strength parameters, including both drained friction angle and undrained cohesion, was determined by automatic averaging from the appropriate CPTU investigations.

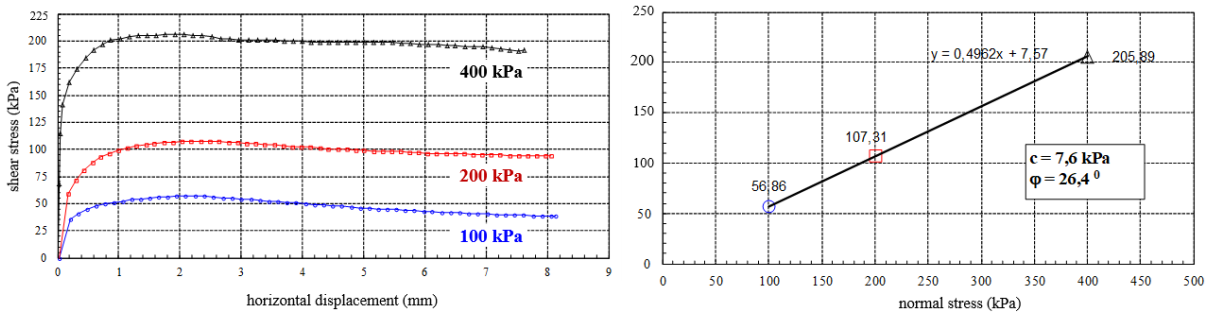

Figure 32 An example of a DSS results for the upper clay layer

An example of averaging the undrained cohesion is given in Figure 33 for one of the CPTs on the location. To ease the overall procedure of soil layering and averaging the strength parameters for relevant layers, an automatic algorithm is developed in Python programming code (Kovačević et al. 2021).

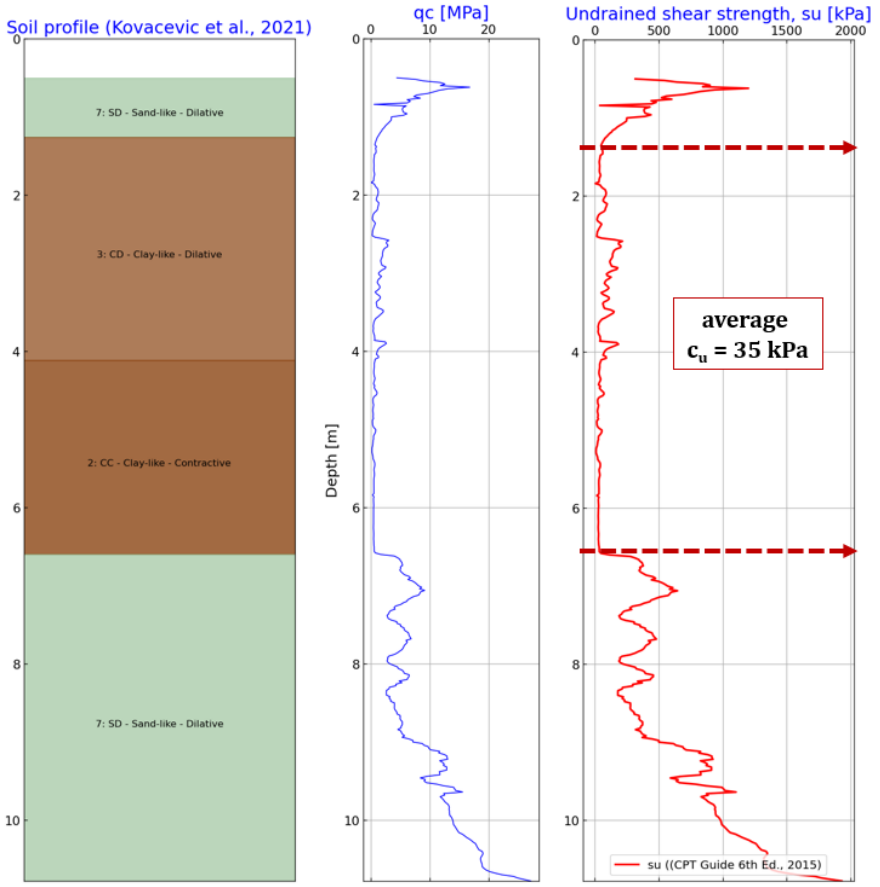

Figure 33 An example of averaging strength parameters from one of CPTs

Table 7 gives the overview of the selected parameters used in the numerical analysis based on which fragility curves were developed. While the unit weight is selected as a deterministic (single) value for each layer and derived from the CPT as suggested by Kovačević et al (2019), strength parameters are selected as mean values (μ) along with Coefficient of Variation (CoV) and standard deviation (σ). Also, strength parameters are defined for both drained and undrained condition.

Table 7: Selected values of drained and undrained parameters for numerical analysis

	unit weight [kN/m³]	**drained parameters**						**undrained parameters**		
		cohesion [kPa]			friction angle [°]			undrained coh. [kPa]		
	deterministic	μ [kPa]	CoV [–]	σ [kPa]	μ [°]	CoV [–]	σ [°]	μ [kPa]	CoV [–]	σ [kPa]
CL	18	8	0,30	2,4	26	0,15	3,9	35	0,30	10,5
SC	19	5	0,25	1,25	31	0,10	3,1	-	-	-

6.3.3 Development of the fragility curves for identified zones

To evaluate the vulnerability of the riverbank slopes, global stability is marked as the relevant failure mechanism, where two types of load are analysed:

a) rapid drawdown:
where for each riverbank section, analysis are performed so that water level external to the riverbank slope experiences a rapid reduction in level to a pre - defined level of a low water (106 m a.s.l), while residual water levels (RWL) in the riverbank remained on higher levels. The fragility curve is defined by varying (decreasing) the RWL in 0.5 m steps. For this analysis, a relative conservative approach is chosen. In reality, and having in mind that the drawdown is occurring through a certain period (not instantaneously), ground water level will also reduce and this dominantly depends on the permeability of the soils forming the riverbank. These analyses are performed using the drained parameters, with 'Effective Stress using B-bar' method. This means that change in pore pressure due to removal of the ponded water will be calculated using the B-bar method.

b) seismic stability:
where during the increase of the pseudo-static loads (acceleration) the probability of stability failure also increases. The maximum considered value of peak horizontal acceleration is selected as 0.3g, which is double the value of the 475-year return period in the city of Karlovac, see Figure 34. These analyses are performed by using drained parameters (first step analyses) and undrained parameters (second step analyses – upper clay modelled with undrained parameters).

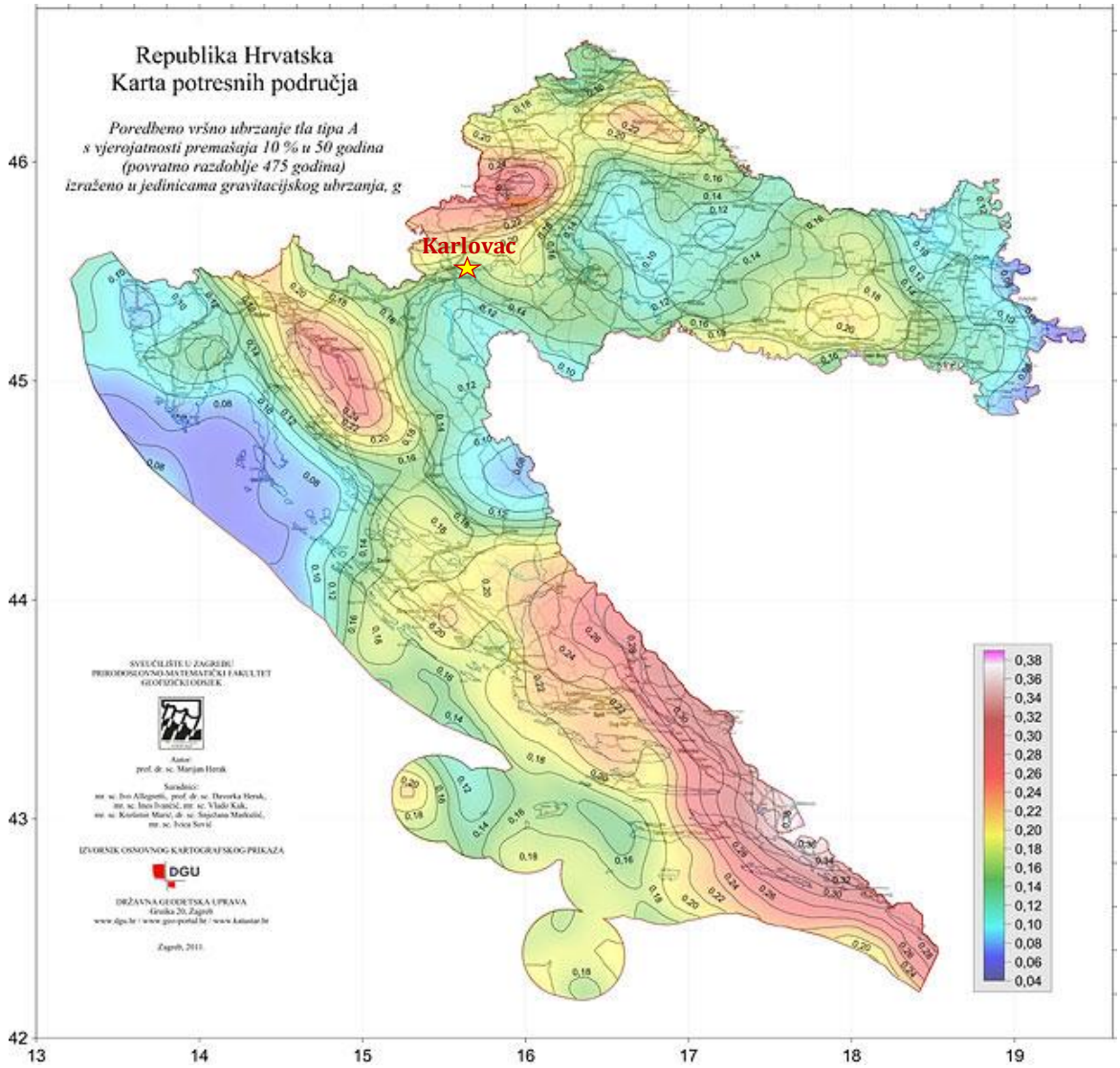

Figure 34 Ground accelerations for 475-year return period in Croatia (obtained from http://seizkarta.gfz.hr)

It should be noted that these two analyses (rapid drawdown stability and seismic stability) are independent, i.e. due to very low probability of their simultaneous occurrence, the analyses are conducted separately. However, seismic analysis were performed for different high water levels, where the water levels are on same height in the riverbank body and external to the slope. Therefore, while the seismic analysis is linked to the certain high-water event, rapid drawdown scenarios are linked to the 'after-high-water' event, since the stability failure occurs after the drawdown of water level external to the slope.

Figures 35 to 42 show the resulting fragility curves for each identified riverbank zone on the right (D) and left (L) side for both rapid drawdown and seismic stability.

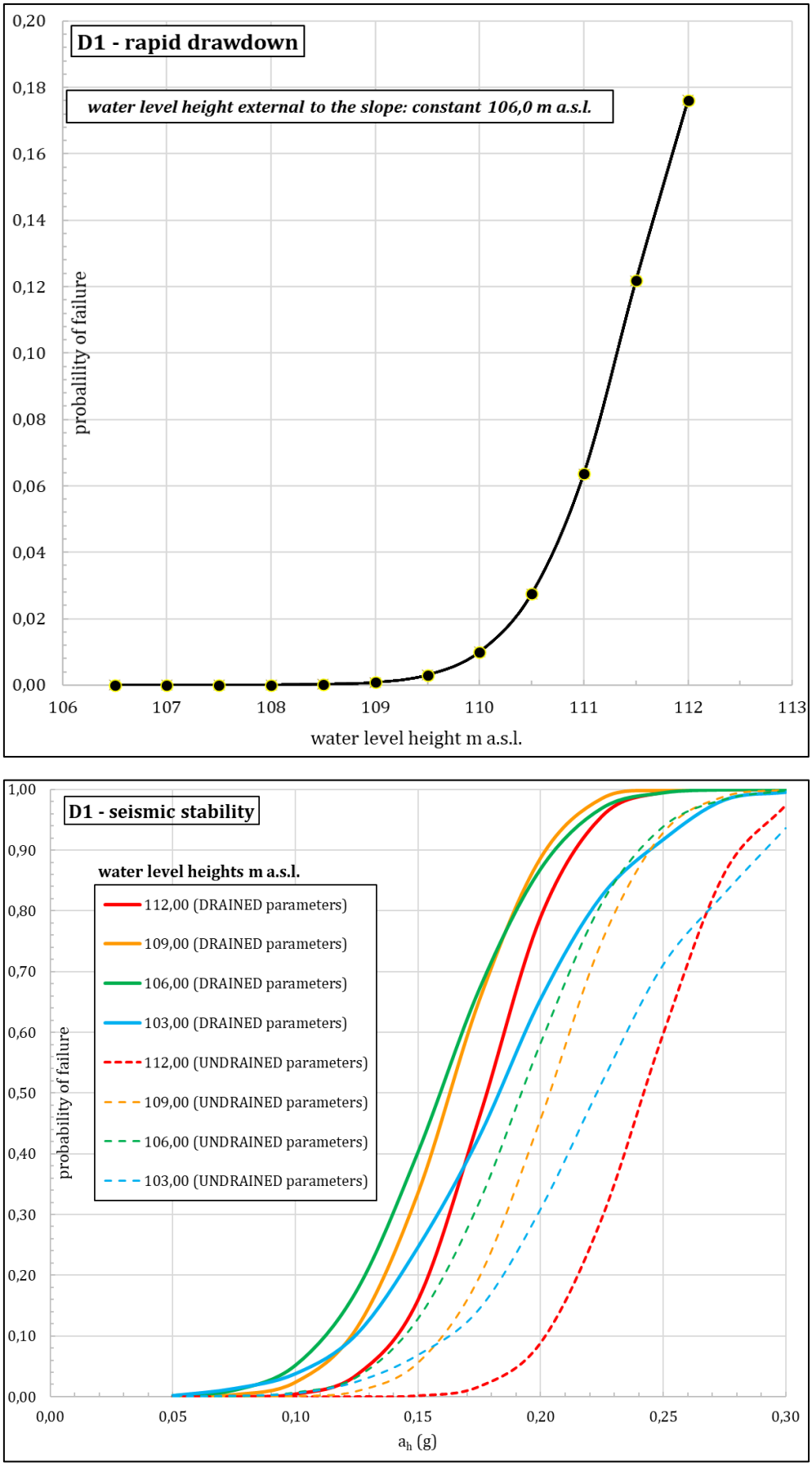

Figure 35 Rapid drawdown (top) and seismic (bottom) fragility curves – zone D1

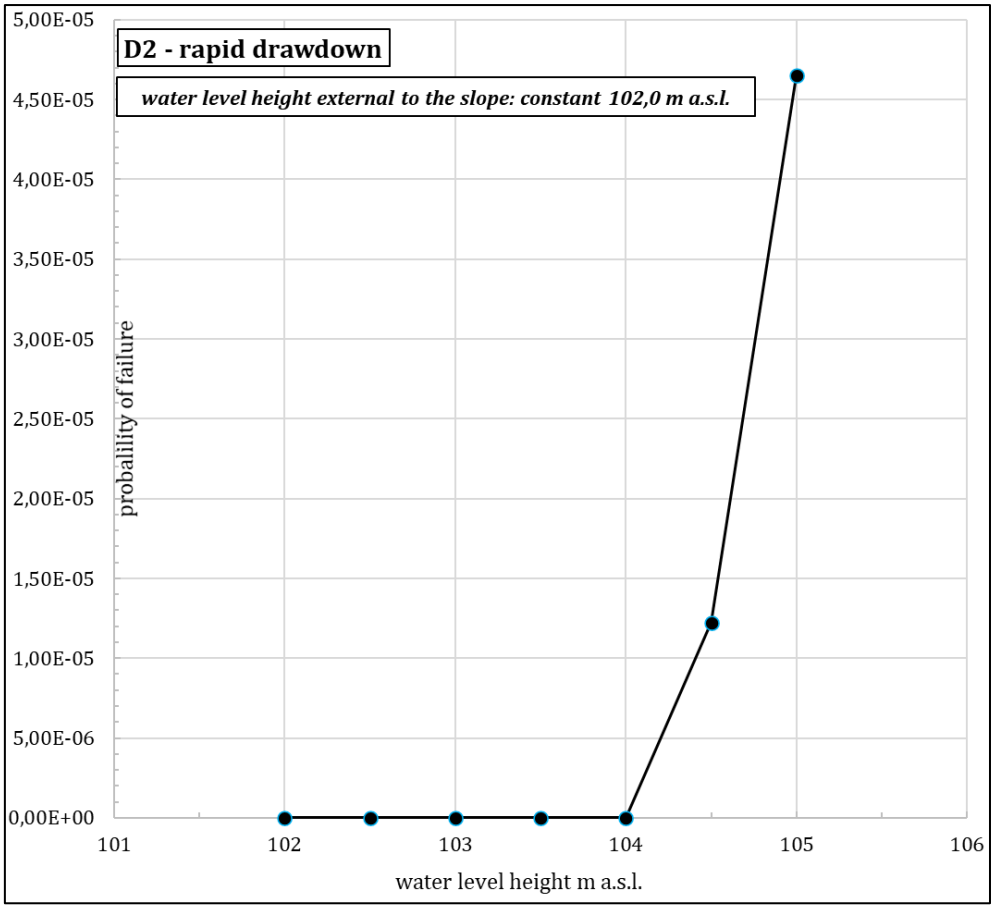

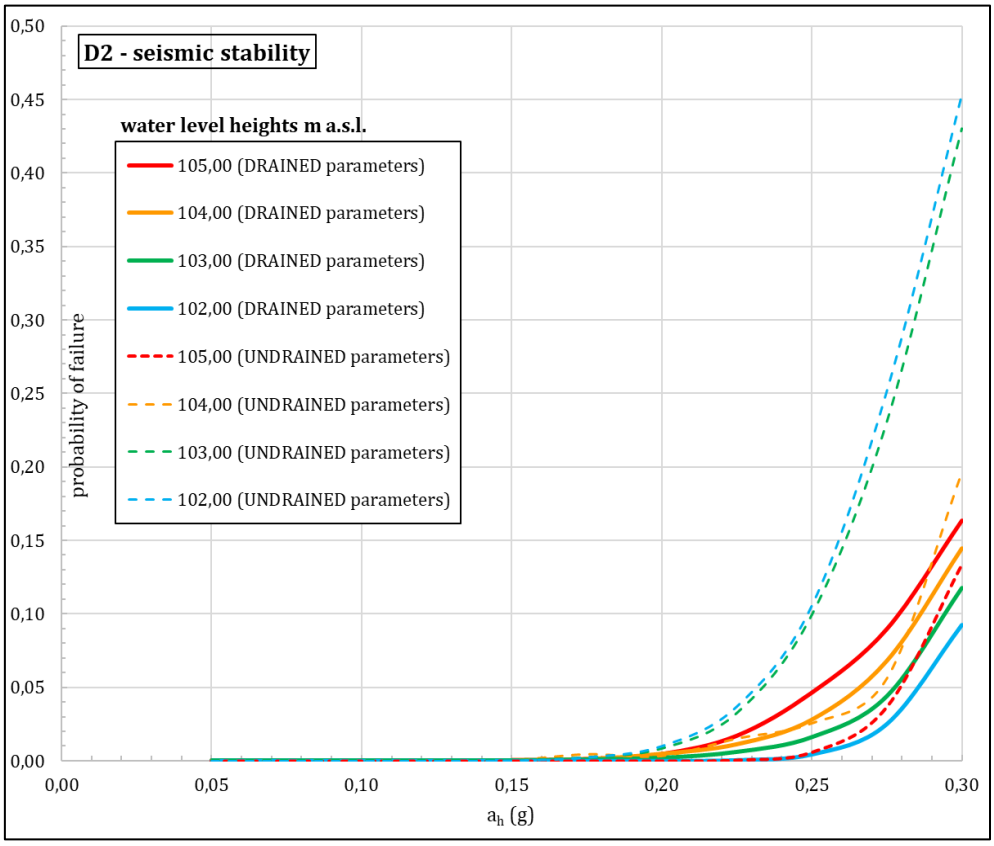

Figure 36 Rapid drawdown (top) and seismic (bottom) fragility curves – zone D2

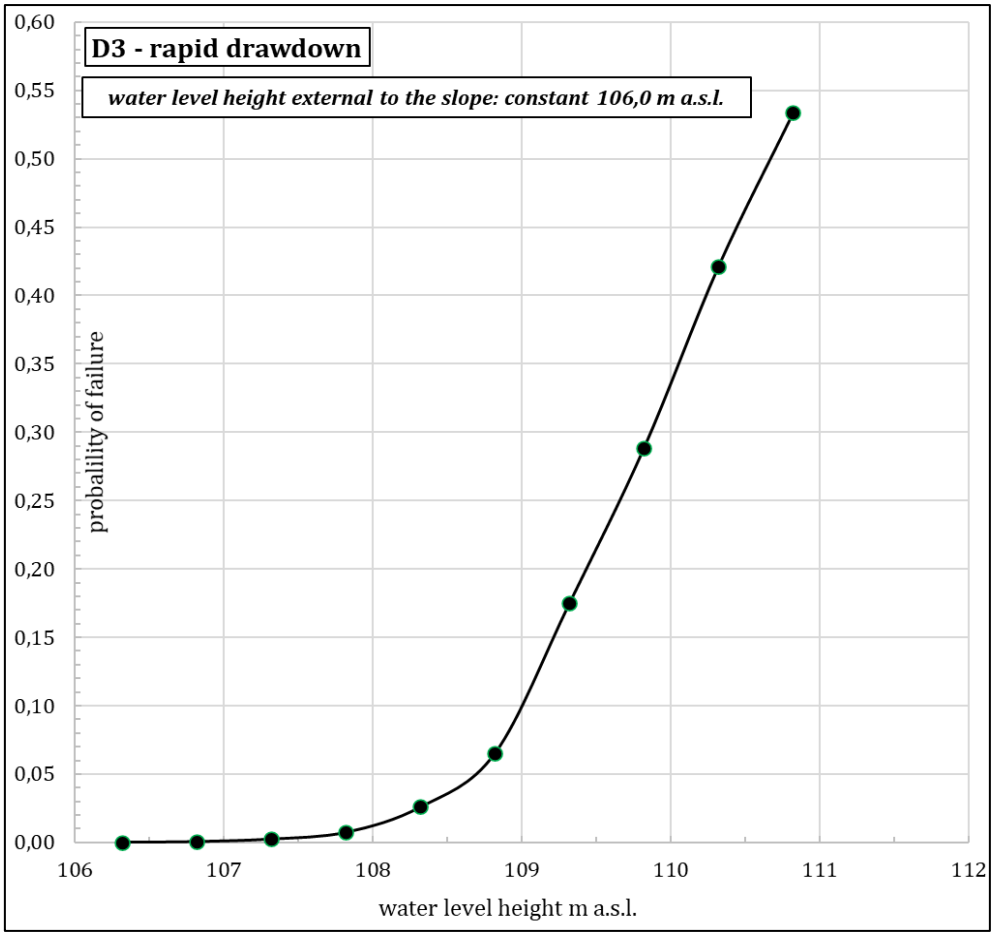

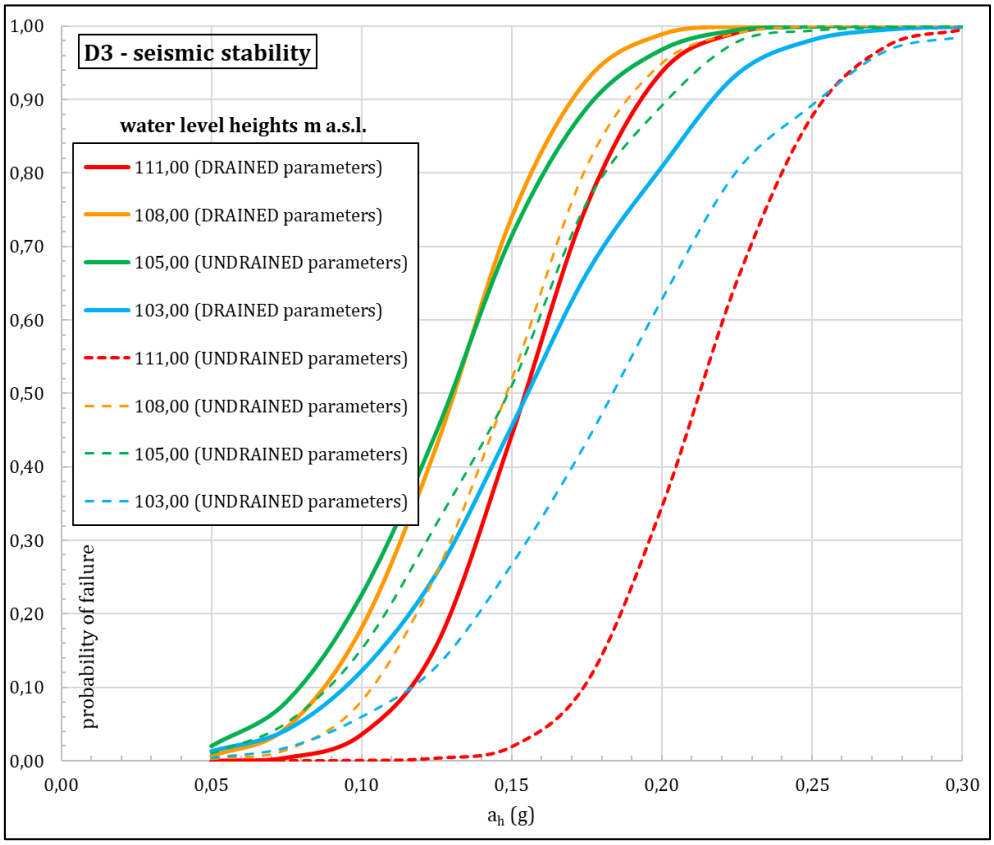

Figure 37 Rapid drawdown (top) and seismic (bottom) fragility curves – zone D3

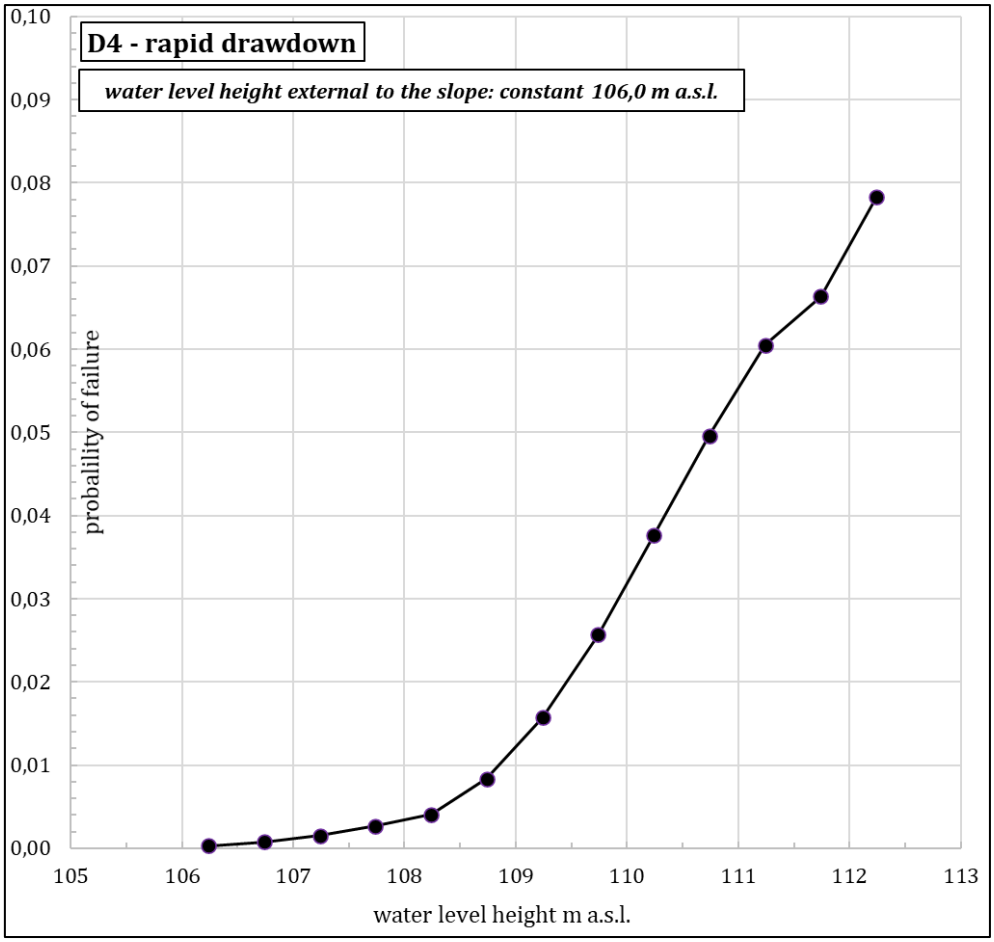

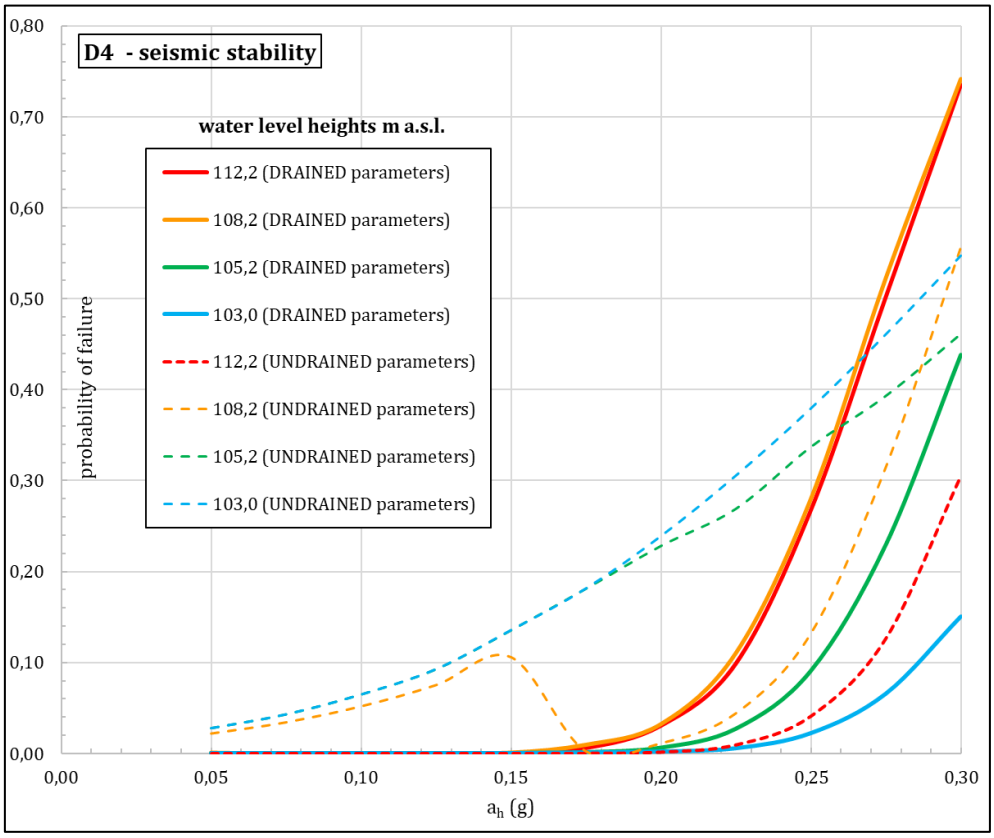

Figure 38 Rapid drawdown (top) and seismic (bottom) fragility curves – zone D4

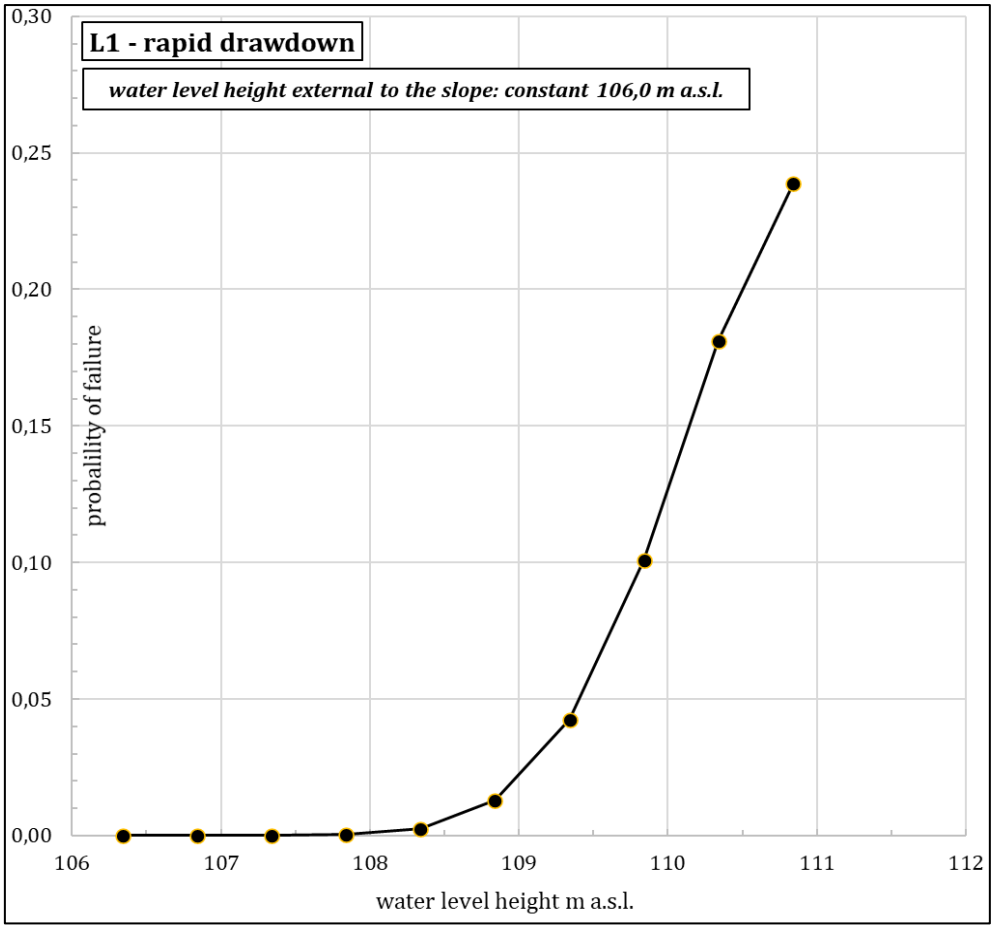

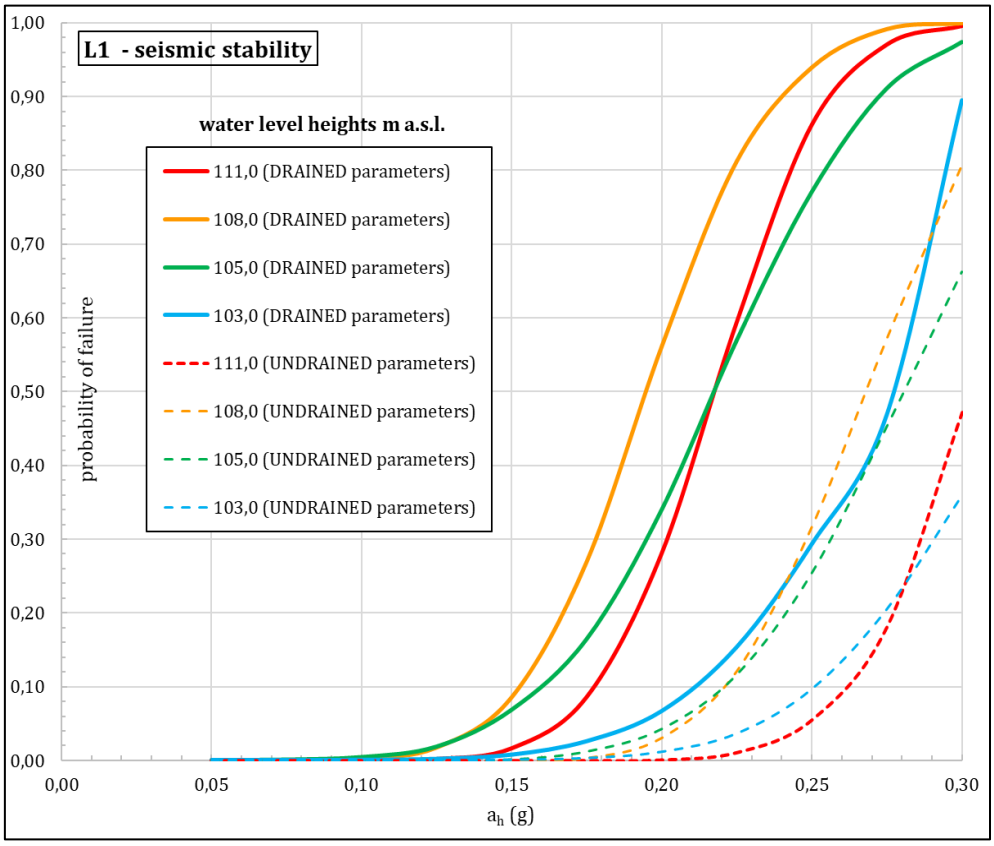

Figure 39 Rapid drawdown (top) and seismic (bottom) fragility curves – zone L1

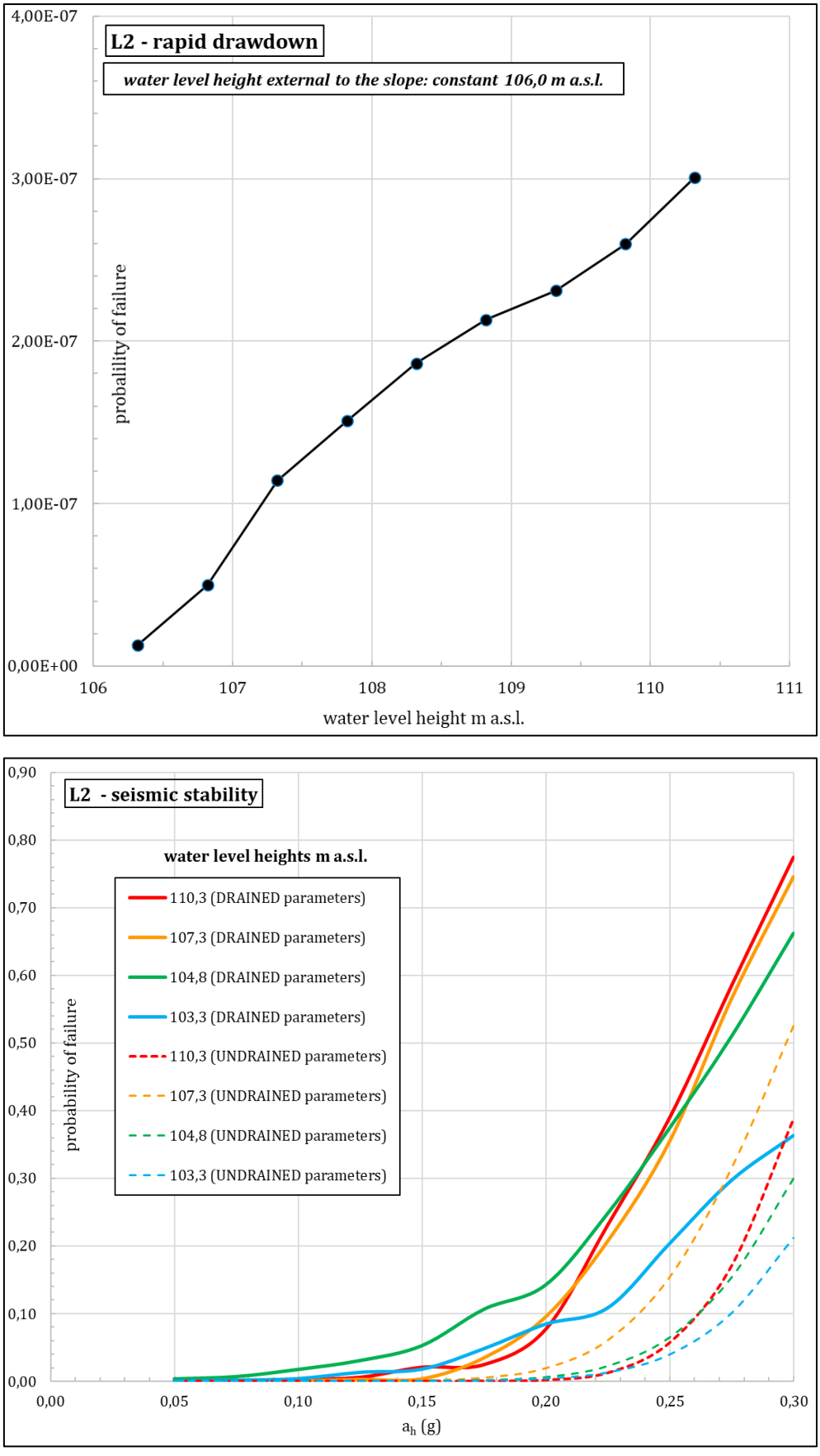

Figure 40 Rapid drawdown (top) and seismic (bottom) fragility curves – zone L2

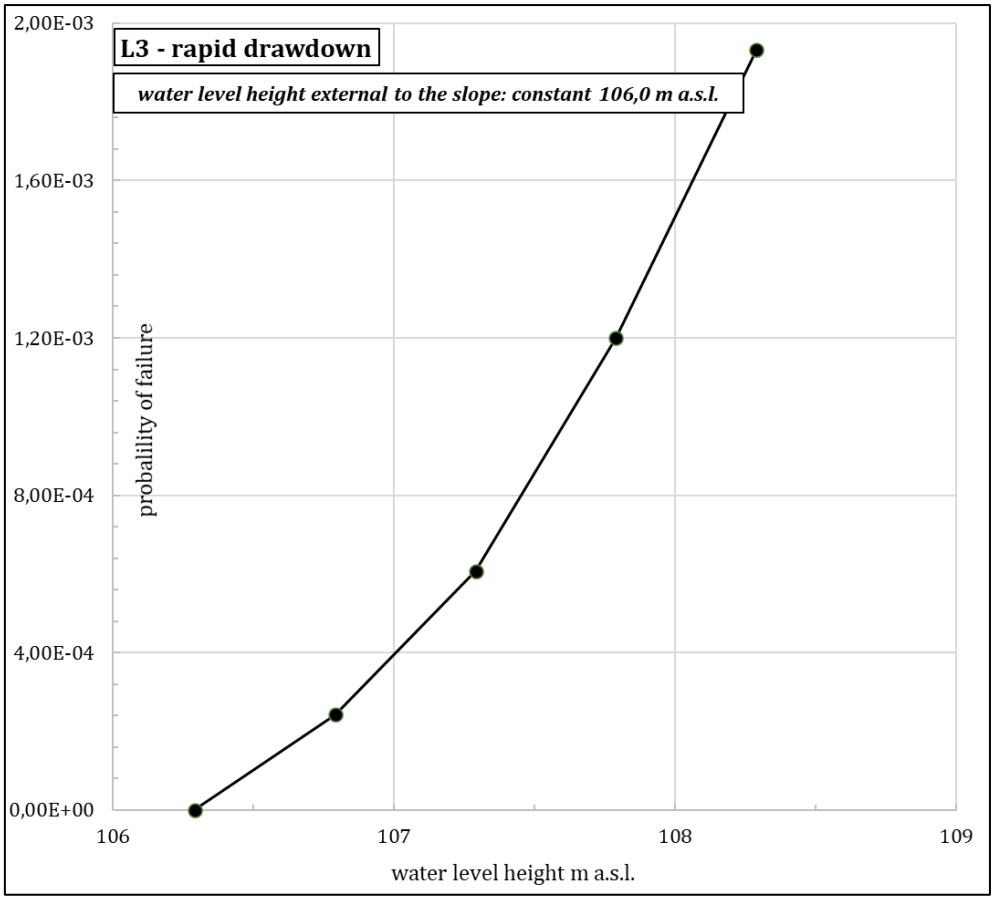

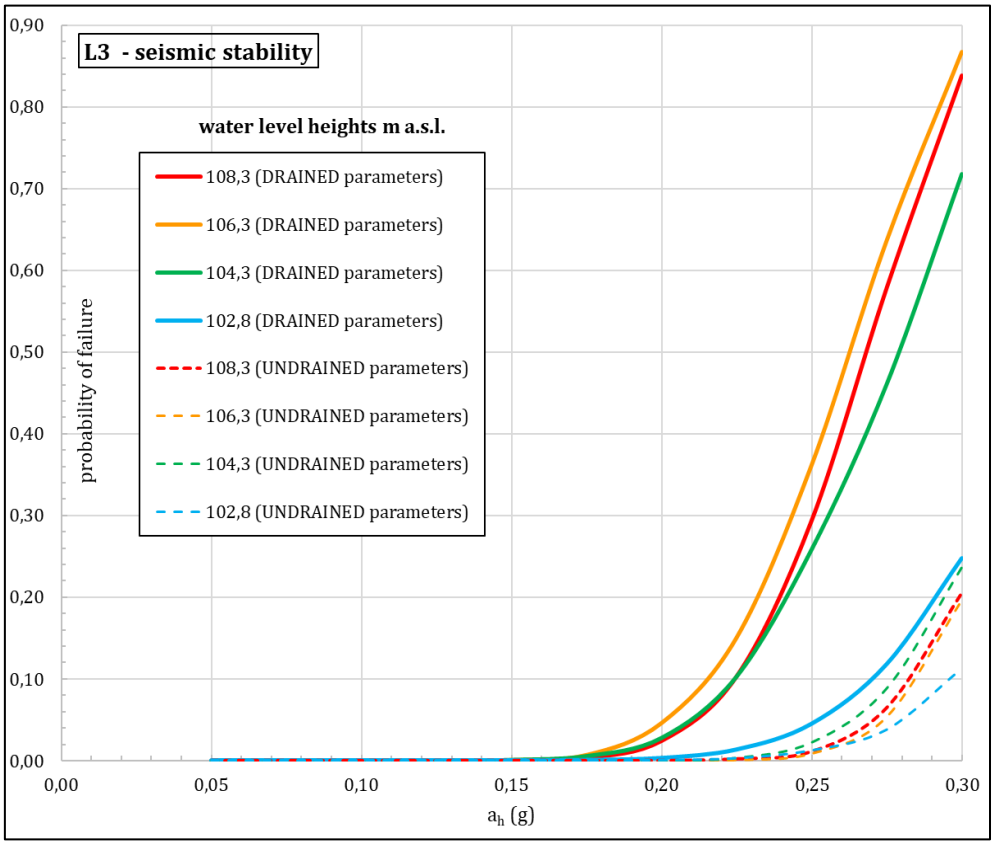

Figure 41 Rapid drawdown (top) and seismic (bottom) fragility curves – zone L3

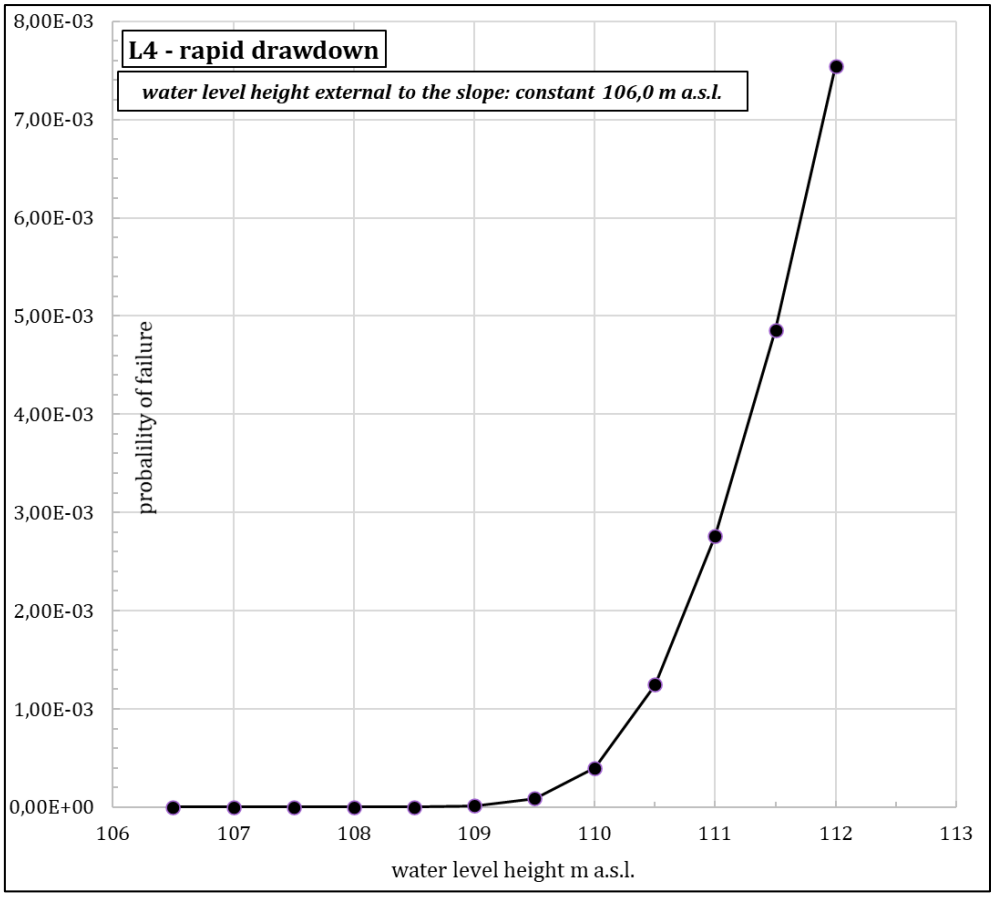

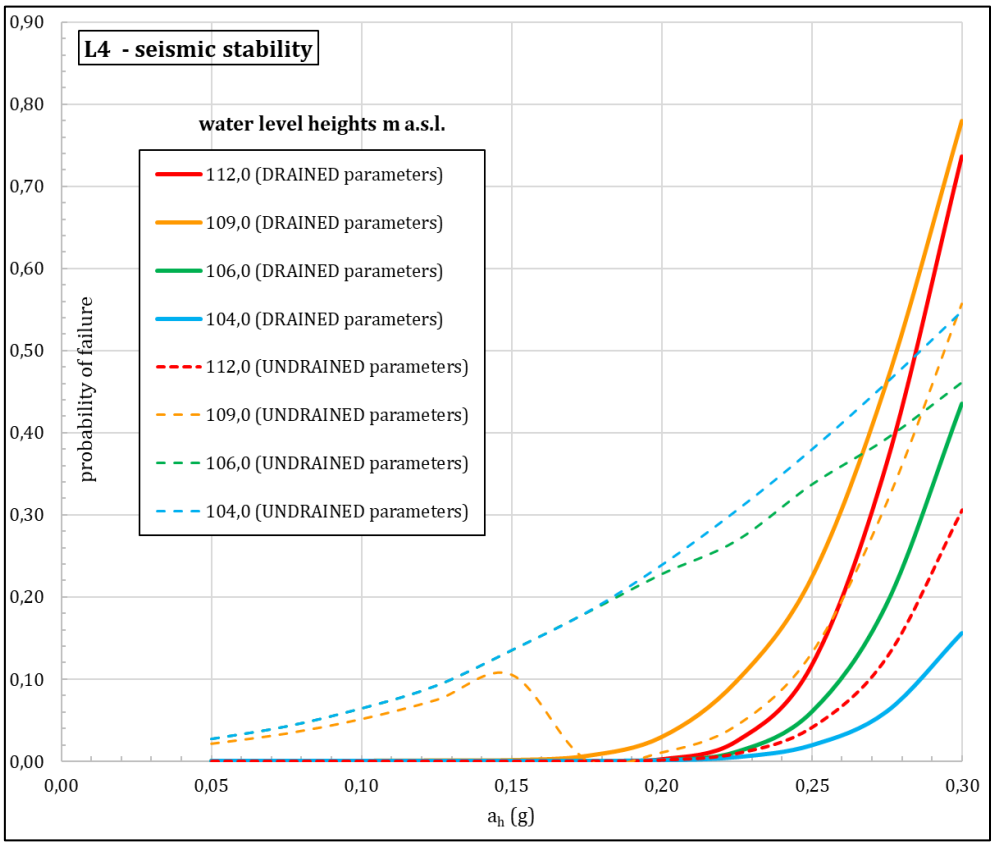

Figure 42 Rapid drawdown (top) and seismic (bottom) fragility curves – zone L4

Presented fragility curves do not take flood return periods into account and as a result the true probability of failure will be lower and dependent on the probability of high water. Tables 8 gives the overview of the probabilities of failure of riverbank for both rapid drawdown (RDD) and seismic scenarios (SS), where for the latter one more critical soil condition (drained / undrained) is stressed - out. For each cross – section, water levels in riverbank (RWL) are defined, as well the water levels external to the riverbank (EWL). For seismic analysis RWL = EWL, while for RDD analysis RWL > EWL. It should be marked that the reference height of Karlovac water level measuring station (reference to deliverable 2.2.) is 103.17 m a.s.l.

Table 8: Overview of the probabilities of failure of riverbank in Karlovac – RDD situation

(**RWL** - residual water level in riverbank; **EWL** – external water level)

Cross section D-1		**Cross section L-1**	
RWL	**RDD p_f (-)** **EWL = 106,0 m a.s.l.**	**RWL**	**RDD p_f (-)** **EWL = 106,0 m a.s.l.**
Top: 112,0 m a.s.l.	0.18	Top: 111,0 m a.s.l.	0.24
109,0 m a.s.l.	7.7×10^{-4}	108,0 m a.s.l.	4.4×10^{-4}
106,5 m a.s.l.	7.3×10^{-6}	106,5 m a.s.l.	1.7×10^{-6}
Cross section D-2		**Cross section L-2**	
RWL	**RDD p_f (-);** **EWL = 102,0 m a.s.l.**	**RWL**	**RDD p_f (-)** **EWL = 106,0 m a.s.l.**
Top: 105,0 m a.s.l.	4.7×10^{-5}	Top: 110,3 m a.s.l.	3.0×10^{-7}
103,0 m a.s.l.	1.5×10^{-8}	107,5 m a.s.l.	1.1×10^{-7}
102,5 m a.s.l.	1.5×10^{-8}	106,5 m a.s.l.	1.3×10^{-8}
Cross section D-3		**Cross section L-3**	
RWL	**RDD p_f (-)** **EWL = 106,0 m a.s.l.**	**RWL**	**RDD p_f (-)** **EWL = 106,0 m a.s.l.**
Top: 111,0 m a.s.l.	0.53	Top: 108,3 m a.s.l.	1.9×10^{-3}
108,0 m a.s.l.	2.6×10^{-2}	107,3 m a.s.l.	6.1×10^{-4}
106,5 m a.s.l.	1.7×10^{-4}	106,5 m a.s.l.	7.3×10^{-11}
Cross section D-4		**Cross section L-4**	
RWL	**RDD p_f (-)** **EWL = 106,0 m a.s.l.**	**RWL**	**RDD p_f (-)** **EWL = 106,0 m a.s.l.**
Top: 112,2 m a.s.l.	7.8×10^{-2}	Top: 112,0 m a.s.l.	7.6×10^{-3}
108,5 m a.s.l.	8.3×10^{-3}	109,0 m a.s.l.	1.4×10^{-5}
106,5 m a.s.l.	2.9×10^{-4}	106,5 m a.s.l.	1.6×10^{-7}

Table 9: Overview of the probabilities of failure of the riverbank in Karlovac – seismic situation

(**RWL** - residual water level in riverbank; **EWL –** external water level)

Cross section D-1			**Cross section L-1**		
RWL = EWL	**SS 0.16g p_f (-)**	**SS 0.30g p_f (-)**	**RWL = EWL**	**SS 0.16g p_f (-)**	**SS 0.30g p_f (-)**
Top: 112,0 m a.s.l.	0.16	1.00	Top: 111,0 m a.s.l.	0.02	1.00
109,0 m a.s.l.	0.35	1.00	108,0 m a.s.l.	0.09	1.00
106,0 m a.s.l.	0.40	1.00	105,0 m a.s.l.	0.07	0.95
103,0 m a.s.l.	0.25	0.99	103,0 m a.s.l.	7.5×10^{-3}	0.90
Cross section D-2			**Cross section L-2**		
RWL = EWL	**SS 0.16g p_f (-)**	**SS 0.30g p_f (-)**	**RWL = EWL**	**SS 0.16g p_f (-)**	**SS 0.30g p_f (-)**
Top: 105,0 m a.s.l.	1.0×10^{-4}	0.16	Top: 110,3 m a.s.l.	0.02	0.78
104,0 m a.s.l.	1.4×10^{-4}	0.19	107,3 m a.s.l.	4.1×10^{-3}	0.75
103,0 m a.s.l.	3.0×10^{-4}	0.43	104,3 m a.s.l.	0.05	0.66
102,0 m a.s.l.	3.6×10^{-4}	0.45	102,8 m a.s.l.	0.02	0.36
Cross section D-3			**Cross section L-3**		
RWL = EWL	**SS 0.16g p_f (-)**	**SS 0.30g p_f (-)**	**RWL = EWL**	**SS 0.16g p_f (-)**	**SS 0.30g p_f (-)**
Top: 111,0 m a.s.l.	0.44	1.00	Top: 108,3 m a.s.l.	2.8×10^{-4}	0.84
108,0 m a.s.l.	0.74	1.00	106,3 m a.s.l.	9.8×10^{-4}	0.87
105,0 m a.s.l.	0.71	1.00	104,3 m a.s.l.	1.4×10^{-3}	0.71
103,0 m a.s.l.	0.46	0.98	102,3 m a.s.l.	6.3×10^{-5}	0.25
Cross section D-4			**Cross section L-4**		
RWL = EWL	**SS 0.16g p_f (-)**	**SS 0.30g p_f (-)**	**RWL = EWL**	**SS 0.16g p_f (-)**	**SS 0.30g p_f (-)**
Top: 112,2 m a.s.l.	1.6×10^{-5}	0.71	Top: 112,0 m a.s.l.	1.6×10^{-5}	0.74
108,2 m a.s.l.	0.10	0.72	109,0 m a.s.l.	0.10	0.78
105,2 m a.s.l.	0.14	0.45	106,0 m a.s.l.	0.14	0.46
103,0 m a.s.l.	0.14	0.53	104,0 m a.s.l.	0.14	0.55

7 Conclusion

This report presented a methodology for developing fragility curves to assess the likelihood of embankment (Netherlands) and riverbank (Croatia) failure. The methodology considered embankment and riverbank failure through global stability (in static and dynamic loading condition), piping, overtopping and rapid drawdown. In the Netherlands where a failure of the dyke would lead directly to flooding, an event tree was used to link the different failure mechanisms while also providing a consistent methodology linking flood return periods to embankment failure. In Croatia, failure of the river bank would not lead directly to flooding.

Two different methods were used to determine the undrained shear strength, the SHANSEP approach adopted in normal Dutch practice for flood defence assessment and a CPT based N_{kt} factor approach. Examining Figure 16 one can see that the characteristic design line from the SHANSEP model gives a lower bound to the in-situ soil strength for near the soil surface but becomes less conservative with depth. While the N_{kt} method describes the mean soil behaviour at the site. The N_{kt} approach was used to generate fragility curves as it allowed for the in-situ variability to be measured and utilised, while the SHANSEP model just considers variability at critical state. By defining the soil conditions at critical strain and over-stressing the soil beyond its pre-consolidation pressure, could remove variability stemming from stress history and potentially affect structure consequently it is likely to underestimate soil variability. It should be noted that the two approaches have only been compared at Oostmolendijk and therefore the comparisons are not definitive. However, at the site the factored SHANSEP method does appear to mask the true soil variability and thus may not always be conservative. A fully probabilistic approach using a mean fit and measured in-situ variability, such as the CPT based approach, would be more prudent when evaluating high risk sites.

At Oostmolendijk, global instability was by far the biggest threat to the dyke system under normal operating conditions, however as flood waters increased in magnitude the likelihood of piping and rapid drawdown failures progressively increased. The system curve shows that for a 1 in 1000 year flood event there is approximately a 1% chance of failure. It should be noted that excessive settlements at the site (which are not considered in the stability assessments), due to the underlying soft layers may cause progressive spreading of the dyke are the most likely driver for the ongoing maintenance works. In our opinion any remedial works that aim to increase the stability of the dyke should be undertaken using light-weight fill materials or other alternative that do not over-stress these very soft soil deposits.

The implementation of the methodology to the Croatian case study included calculating the probability of failure of 3 km of riverbanks on the left and right side of river Kupa. Riverbank stability was assessed for both rapid drawdown and seismic loading scenarios. Characteristic riverbank sections were identified from a photogrammetric survey, and probabilistic calculations performed on each of them.

Calculated values of probability of failure for different scenarios will provide the basis for the classification of the embankments and riverbanks, based on their vulnerability, and

development of an inventory of critical flood protection infrastructure in the case study areas (deliverable 4.3.).

8 References

AHN Viewer (2020). https://www.ahn.nl/ahn-viewer

Bačić, M., Kovačević, M.S. (2021). oVERFLOw Deliverable 3.1: Report on investigation works and monitoring of embankments

Bishop, A. W. (1955) 'The use of the Slip Circle in the Stability Analysis of Slopes', *Géotechnique*, 5(1), pp. 7–17. doi: 10.1680/geot.1955.5.1.7.

Bossenbroek, J.C. (2020) Beoordeling veiligheid primarie waterkingen 2017-2023, Normtraject 17-3 - Oud-Ijsselmonde - Oostendam, Report for the waterschap Hollandse Delta.

Christian, J. T., Ladd, C. C. and Baecher, G. B. (1994) 'Reliability Applied to Slope Stability Analysis', *Journal of Geotechnical Engineering*, 120(12), pp. 2180–2207. doi: 10.1061/(ASCE)0733-9410(1994)120:12(2180).

Espinoza, R. D., Repetto, P. C. and Muhunthan, B. (1992) 'General framework for stability analysis of slopes', *Geotechnique*, 42(4), pp. 603–615. doi: 10.1680/GEOT.1992.42.4.603.

Fredlund, D. G. and Krahn, J. (1977) 'Comparison of slope stability methods of analysis', *Canadian Geotechnical Journal*, 14(3), pp. 429–439. doi: 10.1139/t77-045.

de Gast, T. *et al.* (2020) 'On the reliability assessment of a controlled dyke failure', *Géotechnique*, pp. 1–16. doi: 10.1680/jgeot.19.sip.003.

De Gast, T., Vardon, P. J. and Hicks, M. A. (2020) 'Assessment of soil spatial variability for linear infrastructure using cone penetration tests', *Géotechnique*, pp. 1–15. doi: 10.1680/jgeot.19.sip.002.

Fugro (2020) Geotechnisch Onderzoek, Grondonderzoek primarie waterkingen 2018-2022, 17-3. Document nr. 1318-0180-000, Versie 2, Datum 03/02/2020.

Janbu, N. (1975) *Slope stability computations: In Embankment-dam Engineering. Textbook.*, *International Journal of Rock Mechanics and Mining …*. Edited by Eds. RC Hirschfeld and SJ Poulos. NY: John Wiley & Sons.

Kosič, M., Hekič D., Kalin J., Anžlin A. (2022). oVERFLOw Deliverable 4.2: Fragility curves for embankments subjected to flooding

Kovačević, M.S., Gavin, K.G., Reale, C., Librić, L. (2018). The use of neural networks to develop CPT correlations for soils in northern Croatia, Proceedings of the 4th International Symposium on Cone Penetration Testing (CPT'18), pp. 377-382, 21-22 June, 2018, Delft, The Netherlands, 2018.

Kovačević, M. S., Bačić, M., Librić, L., Žužul, P., Gavin, K., Reale C. (2021). A novel algorithm for vertical soil layering by utilizing the CPT data, Proceedings of 6th International Conference on Road and Rail Infrastructure - CETRA 2020, Lakušić, S. (ed.)., Zagreb: University of Zagreb, Faculty of Civil Engineering, 2021. str. 327-334 doi:10.5592/CO/CETRA.2020.1038

Lacasse, S. *et al.* (2013) 'Reliability of API, NGI, ICP and Fugro Axial Pile Capacity Calculation Methods', in. Society of Petroleum Engineers (SPE). doi: 10.4043/24063-ms.

Ladd, C. and Foott, R. (1974) 'A new design procedure for stability of soft clays', *Journal of the geotechnical engineering division*, 100, pp. 763–786.

Martinović, K., Reale, C. and Gavin, K. (2018) 'Fragility curves for rainfall-induced shallow landslides on transport networks', *Canadian Geotechnical Journal*, 55(6), pp. 852–861. doi: 10.1139/cgj-2016-0565.

Mayne, P. W. (1991) 'Determination of OCR in clays by piezocone tests using cavity expansion and critical state concepts', *Soils and Foundations*, 31(2), pp. 65–76.

Morgenstern, N. R. and Price, V. E. (1965) 'The analysis of the stability of general slip surfaces', *Geotechnique*, 15(1), pp. 79–93. doi: 10.1680/geot.1965.15.1.79.

Phoon, K. and Kulhawy, F. (1999) 'Characterization of geotechnical variability', *Canadian Geotechnical Journal*, 36(4), pp. 612–624.

Newmark, N. M. (1965). Effects of earthquakes on dams and embankments, Geotechnique, 15, pp. 139–159

Prendergast, L. J., Reale, C. and Gavin, K. (2017) 'Probabilistic examination of the change in eigenfrequencies of an offshore wind turbine under progressive scour incorporating soil spatial variability', *Marine Structures*, 57, pp. 87–104.

Reale, C., Xue, J. and Gavin, K. (2017) 'Using Reliability Theory to Assess the Stability and Prolong the Design Life of Existing Engineered Slopes', in *Risk Assessment and Management in Geotechnical Engineering: from Theory to Practice, ASCE Geotechnical Special Publication in Memory of the Late Professor Wilson H. Tang*, pp. 61–81. doi: 10.1061/9780784480731.006.

Rijkswaterstaat (2014) *The National Flood Risk Analysis for the Netherlands,*.

Robertson, P. (1990) 'Soil classification using the cone penetration test', *Canadian Geotechnical Journal*, 27(1), pp. 151–158.

Rossi, N. *et al.* (2021) 'Development of Fragility Curves for Piping and Slope Stability of River Levees', *Water 2021, Vol. 13, Page 738*, 13(5), p. 738. doi: 10.3390/W13050738.

Santamarina, J. (1992) *Reliability of slopes: Incorporating Qualitative Information (ABRIDGMENT)*, *Transportation Research Board*. Transportation Research Board.

Spencer, E. (1967) 'A method of analysis of the stability of embankments assuming parallel inter-slice forces', *Geotechnique*, 17(1), pp. 11–26.

Terzhagi, K. (1950). Mechanism of landslides, Application of Geology to Engineering Practice (Berkey Volume), Geological Society of America, S. Paige (Ed.), New York), pp. 83-123.

URL: http://seizkarta.gfz.hr (accessed on February 5th 2022)

US Army Corps of Engineers (1999) *Risk based analysis in geotechnical engineering for support of planning studies, engineering and design*.

Whitman, R. (2000) 'Organizing and evaluating uncertainty in geotechnical engineering', *Journal of Geotechnical and Geoenvironmental Engineering*, 126(7), pp. 583–593. doi: http://dx.doi.org/10.1061/(ASCE)1090-0241(2000)126:7(583).